nature reviews genetics

https://doi.org/10.1038/s41576-023-00611-y

Review article

Check for updates

microRNAs in action: biogenesis, function and regulation

Renfu Shang, Seungjae Lee, Gayan Senavirathne & Eric C. Lai

Abstract

Ever since microRNAs (miRNAs) were first recognized as an extensive gene family >20 years ago, a broad community of researchers was drawn to investigate the universe of small regulatory RNAs. Although core features of miRNA biogenesis and function were revealed early on, recent years continue to uncover fundamental information on the structural and molecular dynamics of core miRNA machinery, how miRNA substrates and targets are selected from the transcriptome, new avenues for multilevel regulation of miRNA biogenesis and mechanisms for miRNA turnover. Many of these latest insights were enabled by recent technological advances, including massively parallel assays, cryogenic electron microscopy, single-molecule imaging and CRISPR–Cas9 screening. Here, we summarize the current understanding of miRNA biogenesis, function and regulation, and outline challenges to address in the future.

Sections

Developmental Biology Program, Sloan Kettering Institute, New York, NY, USA. e-mail: laie@mskcc.org

Introduction

It has been 30 years since curiosity-driven research into *Caenorhabditis elegans* development yielded the first insights into microRNAs (miRNAs)[1,2], and their general regulatory and targeting principles were evident from *Drosophila* molecular genetic studies[3–5] even before knowledge of miRNAs in this species[6]. In 2001, miRNAs were recognized as a broad class of small RNAs across higher eukaryotes[7–9], triggering intense research into this new regulatory paradigm across scientific disciplines. The next decade revealed major catalogues of conserved miRNA loci, molecular factors central to miRNA biogenesis and function, and their regulatory mechanisms.

miRNAs are RNAs ~22 nucleotides in length that derive from longer primary miRNA (pri-miRNA) transcripts, which bear one or more hairpins (Fig. 1a). Most miRNA hairpins derive from non-coding transcripts or introns; few overlap exons of protein-coding genes. Most conserved miRNAs (that is, shared across vertebrates) are generated through a canonical pathway involving two RNase III enzymes[10] (Fig. 1a). First, the hairpin base of a pri-miRNA transcript is 'cropped' by the nuclear Microprocessor complex, comprising one RNase III Drosha molecule bound to two copies of its partner DGCR8, releasing a precursor miRNA (pre-miRNA) hairpin ~55–70 nucleotides in length. The pre-miRNA is exported to the cytoplasm and cleaved near the terminal loop by the RNase III Dicer, yielding a miRNA duplex that can interact with a member of the Argonaute (Ago) protein family. Following discard of the miRNA* species (also known as the passenger strand), a process governed by sequence and structural features of the duplex, the mature single-stranded miRNA guides the Ago complex to repress complementary RNA targets[11]. Additional non-canonical miRNA pathways exist that are Drosha-independent (Fig. 1b) and/or Dicer-independent[12] (Fig. 1c). Knowledge of such atypical pathways enables the design of synthetic substrates that efficiently bypass both RNase III enzymes to generate functional miRNAs[13,14].

Although various modalities of miRNA–target pairing have been proposed, repression of metazoan mRNAs almost always involves 'seed' pairing to nucleotides 2–8 of the miRNA[6,15–17]. Argonaute–miRNA–target structures reveal a structural basis for such pairing, as the miRNA seed is pre-arranged into an A-form conformation that is primed for base-pairing with its target mRNA[18–20]. Repression of seed-matched targets is mediated by the Ago adapter GW182 (TNRC6), which recruits additional factors for mRNA degradation and/or translational repression. All four mammalian Ago proteins regulate seed-matched targets, but Ago2 uniquely exhibits the ability to use endogenous miRNAs and synthetic small RNA guides to cleave extensively paired targets[21,22], an activity that does not require cofactors and mediates experimental RNA interference (RNAi). Under specific circumstances, Ago3 can also cleave targets[23,24], although the biological significance of this requires further study.

These core aspects of miRNA biogenesis and function were revealed using traditional biochemistry, molecular genetics and cell biology approaches, along with deep sequencing and X-ray crystallography. Catalysed by recent technical innovations and experimental strategies, including high-throughput substrate assays, cryogenic electron microscopy (cryo-EM), single-molecule approaches and CRISPR screening, the last decade has witnessed the emergence of novel insights into miRNA pathways. Here, we review the application of these techniques to the miRNA pathway (Table 1). Although we focus on recent work in mammalian systems, research across diverse species has and continues to be foundational, and we highlight relevant miRNA research from non-mammalian organisms throughout.

High-throughput miRNA assays

Until recently, direct experimental tests of miRNA biogenesis and function involved small to medium-scale assays, such as in vitro processing of specific miRNA substrates, and reporter assays of variant miRNA–target pairing configurations. Genomic profiling, such as small RNA sequencing or transcriptome measurements, inherently yields broad information. However, endogenous data sets have limitations for interpretation, including a panoply of indirect effects and the inability to query cell-specific loci, and limited ability to assay synthetic variants. Overcoming these challenges, creatively designed massively parallel substrate processing assays and Ago binding assays (Fig. 2a) have enabled new insights into miRNA biogenesis and target regulation.

Features of Drosha (pri-miRNA) substrates and cleavage

As a gatekeeper for RNA transcripts entering the canonical miRNA pathway (Fig. 1), pri-miRNA surveillance provides the first checkpoint for miRNA substrate selection[25]. Early assays of pri-miRNA variants demonstrated the importance of general structural features, including a double-stranded stem of ~35 bp, flanking single-stranded sequences and a single-stranded terminal loop of ≥10 nucleotides[26–29] (Fig. 2b). However, these features are insufficient to discriminate genuine miRNA hairpins amongst millions of seemingly comparable hairpins from RNA secondary structure predictions, suggesting other determinants.

High-throughput miRNA processing assays enable systematic discovery of sequence and structural features within functional miRNA substrates. Specific pri-miRNAs can be used as a foundation for large variant pools, which are then subjected to in vitro cleavage using cell lysate or purified Microprocessor (Fig. 2a). The processed products are purified, sequenced and compared with the initial pool to determine preferred features of effective pri-miRNA substrates. Initial assays recapitulated general features of the effective pri-miRNA substrates mentioned above and revealed novel attributes such as UG in the 5′ basal junction, UGU/GUG in the apical junction, CNNC in the 3′ flanking region[30] and a mismatched GHG (mGHG) motif in the lower stem[31] (Fig. 2b). Some of these motifs were suspected to be recognized by Drosha or DGCR8 (see also structural studies below). For example, hemin (an Fe^{3+}-bound porphyrin, distinct from haem which is an Fe^{2+}-bound porphyrin) enhances the interaction between the DGCR8 dimer and the apical loop, especially with the UGU motif, to ensure efficiency and fidelity of pri-miRNA cleavage[32,33]. Other motifs revealed new molecular players, such as the recognition of 3′ CNNC by SRSF3, which aids proper positioning of Microprocessor[30,34,35]. Additional features include how mismatches, wobble base pairs and bulges in the upper stem of pri-miRNA hairpins can influence Microprocessor efficiency and accuracy[36,37]. Notably, the overall hairpin structure remains central to efficient cleavage of pri-miRNAs, and no primary motif seems essential. However, this 'menu' of motif features can compensate or enhance miRNA biogenesis when the pri-miRNA lacks optimal structural features[31]. Reciprocally, knowledge of optimal pri-miRNA backbones can improve designs for highly efficient RNAi vectors[31,38].

More recently, comprehensive pri-miRNA processing assays involving a large number of endogenous pri-miRNAs, in vitro[39,40] or in cells[41], evaluated the processing efficiency and accuracy in greater quantitative detail. These studies echoed earlier smaller-scale assays[42] in revealing that numerous pri-miRNAs in the miRBase registry[43] were not processed above background[40,41], and may be false entries[44]. Still, both in vitro and transfected assays have their own limitations, as robust in vitro microprocessing may not fully recapitulate aspects

of in vivo regulation. In addition, assays of transfected plasmids do not mimic normal genomic or chromatin context. An open question from these studies arises from the fact that in vitro cleavage of pri-miRNA hairpins reveals aberrant products, such as nicked hairpins or inverted processing[40,45]. It remains unclear whether these aberrant products are in vitro artefacts or biochemically valid activities that require suppression in vivo.

Features of Dicer (pre-miRNA) substrates

General features of pre-miRNA hairpins that enable Dicer cleavage emerged from in vitro and in vivo mutational studies of endogenous and synthetic pre-miRNAs. An optimal pre-miRNA usually contains a 5′-end monophosphate, a 3′-end two-nucleotide overhang, a double-stranded stem of >20 bp and a single-stranded terminal loop[46]. These features are incorporated into several different models of dicing control (Fig. 2c).

Initial studies revealed that Dicer uses its PAZ domain to recognize the 3′-dinucleotide overhang and measure ~21–25 nucleotides (depending on the species) to cleave the double-stranded RNA (dsRNA) stem and release the small RNA duplex[47–51]. This so-called 3′-counting rule emphasized 'ruler'-like activity of Dicer to cut at a prescribed distance from the 3′ substrate terminus. Subsequent work revealed a 5′-counting rule, whereby human Dicer can also recognize the 5′ phosphorylated end of the pre-miRNA hairpin and cleave the hairpin stem ~22 nucleotides from the 5′ end[52]. Notably, it is not clear how Dicer selects different counting rules for different miRNA substrates. Finally, the distance between the 5′ end of miRNA-3p species and the adjacent bulge or loop in the pre-miRNA hairpin influences the Dicer cleavage site, termed the loop-counting rule[53]. When this distance is two nucleotides, Dicer preferentially cuts precisely at the 5′ end of miRNA-3p. Distances other than two nucleotides lead to heterogeneous Dicer cleavage, yielding multiple miRNA isoforms (Fig. 2c).

Massively parallel substrate assays confirm these features and reveal new ones. For instance, recent large-scale assays of pre-miRNA variants revealed a conserved GYM motif (paired G, paired pyrimidine and mismatched C or A) near the cleavage site of human Dicer. The GYM motif is recognized by the double-stranded RNA-binding domain (dsRBD) of Dicer and can override other counting rules for dicing[38]. Another study of 20,000 pre-miRNA variants showed that a single-nucleotide bulge near the terminal loop on the 3′ arm (22-bulge) can promote pre-miRNA dicing and enhance gene silencing[54] (Fig. 2c). Ultimately, comprehensive knowledge of combined Microprocessor and Dicer substrate features may permit effective bioinformatic prediction of canonical miRNAs directly from individual genomes, that is, without considering phylogenetic conservation. This remains an enticing challenge, and deep learning methods may bring us closer to the goal of recapitulating in silico what a cell does quite naturally.

Comprehensive analysis of Argonaute targeting

The functional Ago complex, sometimes referred to as the single-stranded guide RNA-induced silencing complex (RISC), identifies targets via base-pairing of loaded RNA (Fig. 2d). The most abundant miRNA target sites (canonical sites) contain six or seven contiguous base pairs between the miRNA seed region (preferentially nucleotides 2–8 of the miRNA) and its target mRNA[6,16] (Fig. 2d). Such minimal matching to miRNA 5′ ends is necessary and often sufficient for target regulation[15,17]. Activity of the seven-nucleotide seed match is enhanced by a target adenosine opposite the first miRNA position (t1A). miRNAs usually begin with U, which appears to base-pair with t1A (Fig. 2d). However, as the miRNA 5′ base is bound by the specificity loop in the Ago MID domain[55,56], it is not actually available for pairing[19,20]. Instead, Ago proteins exhibit intrinsic binding preference for miRNA 5′-U, and possess a solvated surface pocket that specifically binds t1A (ref. 57).

Some canonical sites contain additional base-pairing, although this does not necessarily enhance silencing. However, rare non-canonical sites lacking six contiguous seed matches can be compensated by extensive 3′ base-pairing (positions ~13–16), a phenomenon termed supplemental or 3′-compensatory pairing[10] (Fig. 2d). Other examples of non-conventional miRNA targeting include extensively 'centred' base-pairing[58], and certain variations of interrupted seeds[59,60] (Fig. 2d). Furthermore, other putative, non-canonical miRNA–target pairing interactions have been reported from Ago-CLIP and reporter studies[59–62]. In general, it is unclear whether non-seed miRNA–target interactions can be reconciled with structural data of Argonaute regulatory complexes. To address this more systematically, large-scale assays are critical. One study used high-throughput imaging-based assays to assay the binding energies, association and cleavage rates of 40,000 target site variants for two miRNAs (let-7a and miR-21)[63]. This work revealed some distinctions in the behaviour of individual miRNAs, likely attributable to different G/C content in the seed region. Ago RNA bind-n-seq (RBNS) assays were also applied[64]. In such experiments, purified complexes of Ago2 loaded with an individual miRNA were incubated with large random RNA oligo pools, and bound targets were sequenced to infer binding affinities (Fig. 2a). Testing different concentrations of Ago2–miRNA complex with RBNS showed that binding to different site types was dependent on the concentration of the Ago2–miRNA complex, and detected binding idiosyncrasies of specific miRNAs. Whereas expected classes of seed-based matches correlated with binding efficacy and regulation, non-canonical sites were documented with certain miRNAs, although these tended to be of low affinity and did not reliably confer repression in functional sensor assays in cells. Overall, miRNA–target site binding affinity is the major determinant of miRNA-mediated target repression[64], but 3′ pairing can have substantial effects depending on the miRNA sequence[65].

Local features such as flanking AU-rich dinucleotides and structural availability of the miRNA target site can enhance or enable Ago binding. In addition, miRNA-mediated repression is strongly enhanced when sites reside in 3′ untranslated regions (UTRs), which is attributable to dislodging of Ago complexes by translocating ribosomes[66,67]. However, coding sequence (CDS) sites can be functional, especially in the vicinity of rare codons[67] or within CDS repeats[68]. Another variation was reported for atypical CDS sites lacking seed matches but with 3′-compensatory pairing[69]. This configuration was concluded to operate in a GW182-independent manner to repress translation by inducing transient ribosome stalling. Although the endogenous regulatory contribution of such sites remains unclear, 3′-only pairing configurations were detected in Ago2-RBNS with select miRNAs[64].

miRNA modification can also modulate target binding. The most frequent 3′ non-templated addition of miRNAs is uridine[70], which may enhance 3′ supplemental pairing to certain sites. For example, a non-functional miR-27a site with limited seed match is responsive to 3′-uridylated miR-27a, which extends pairing with adenosine in the target[71]; this phenomenon was termed tail-U-mediated repression (TUMR). This is consistent with evidence that a lengthened miRNA 3′ end can lead to expanded and stronger 3′ supplementary pairing interactions[72]. Reciprocally, miRNAs can be trimmed from their 3′ ends.

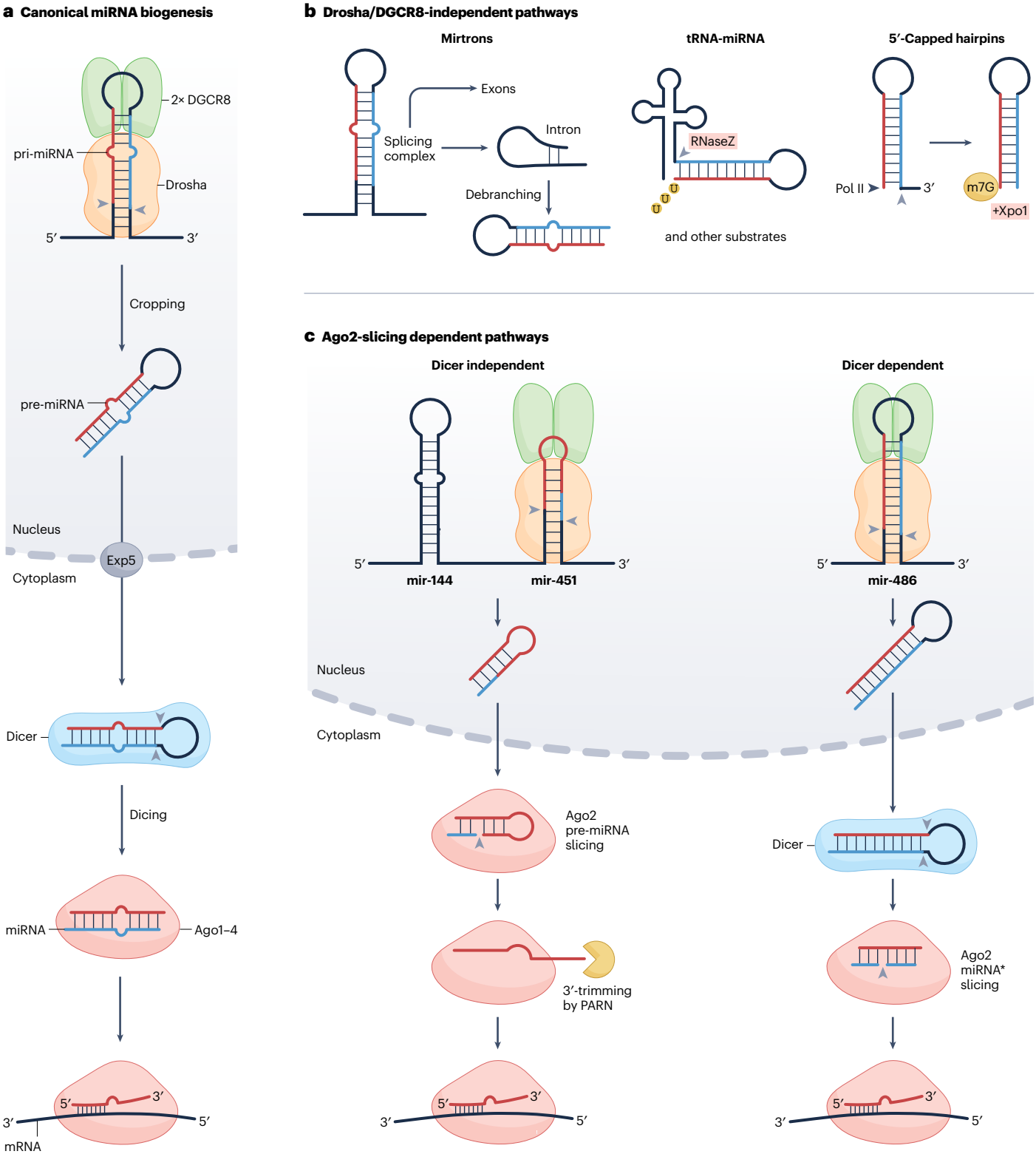

A new study reports that under high Mn^{2+} conditions, 3′ exonucleases including ISG20, TREX1 and ERI1/3′hExo can execute extreme trimming of Ago-loaded miRNAs into tiny RNAs of ~14 nucleotides[73] (Fig. 2e). Moreover, certain miRNA-derived tiny RNAs can activate cleavage activity of Ago3. Although the in vivo significance of this mechanism remains to be determined, high Mn^{2+} conditions during stress or viral

Fig. 1 | Canonical and non-canonical miRNA biogenesis pathways. a, Canonical microRNA (miRNA) biogenesis. A primary miRNA (pri-miRNA) transcribed by RNA polymerase II (Pol II) is cleaved in the nucleus by Microprocessor (Drosha–DGCR8). The resulting precursor miRNA (pre-miRNA) is exported to the cytoplasm by Exportin 5 (Exp5), a member of the nuclear transport receptor family. Once there, Dicer cleaves the terminal loop to yield a miRNA duplex that is loaded into an Argonaute (Ago) protein. After removal of the passenger strand (blue), the single-stranded mature miRNA (red) guides the functional Ago effector complex (now termed RNA-induced silencing complex (RISC)) to silence complementary RNA targets. Cleavage sites are denoted by grey arrowheads. **b**, Non-canonical mechanisms of miRNA biogenesis, involving the generation of pre-miRNA hairpins independent of Microprocessor. Left: mirtrons are pre-miRNA mimics generated by the splicing machinery and intron-debranching enzymes, thereby bypassing Microprocessor[216,217]. Middle: MHV (murine hepatitis virus) tRNA biogenesis via RNase Z (grey arrowhead) can liberate functional pre-miRNAs[218]. Right: RNA Pol II transcription can directly yield pre-miRNAs bearing a 5′-cap (m^7G), which are exported to cytoplasm by XPO1, as exemplified by the *mir-320* family. Because Ago binding requires 5′-monophosphate, Dicer cleavage of capped pre-miRNA hairpins yields mature miRNA only from 3′ arms[219,220]. Additional non-canonical miRNA biogenesis strategies have been described (not shown). **c**, Ago2 cleavage-dependent miRNAs. Most miRNAs do not require catalytic activity of Ago2 for biogenesis, but two conserved exceptions are known. Left: *mir-451* has a short hairpin stem (18 bp) that cannot be cleaved by Dicer. Instead, following cleavage of its primary transcript by Microprocessor, the *pre-mir-451* hairpin is directly bound and cleaved (sliced) by Ago2, followed by 3′ resection via poly(A)-specific ribonuclease (PARN) to generate mature miR-451 (refs. 221–223). Right: *mir-486* bears perfect base-pairing in its pre-miRNA stem and requires not only Drosha and Dicer to produce a miRNA duplex but also cleavage of the passenger strand (miRNA*) by Ago2 to yield the mature single-stranded RISC[149].

infection could plausibly alter miRNA activity. Finally, the local binding of RNA-binding proteins (RBPs), including HuR, Pumilio, DND1 and, potentially, many others, can affect miRNA site efficacy[74–77].

These scenarios indicate why in vitro affinity of Ago2–miRNA–target ternary complexes might not capture the totality of in vivo Ago-mediated regulation. Conversely, it is important to recognize that many proposed unconventional target sites confer subtle or undetectable regulation. As CRISPR mutations of endogenous miRNA target sites are now straightforward to install, it will be critical to use this approach to evaluate whether atypical sites (as well as canonical seed matches) directly mediate in vivo miRNA silencing and/or phenotypically relevant biology.

Insights from RNase III cryo-EM structures

The typically precise sequences of mature miRNAs that are hewn from long primary transcripts suggest that the stereotypical actions of Drosha and Dicer involve ruler-like measurements. Similarly, the characteristic seed region of miRNAs that is predominantly required for targeting implies specific structural constraints on the ternary Ago–miRNA–target complex. These were inferences from the initial structures of Dicer and Argonaute homologues from protozoan (*Giardia intestinalis*) and archaeal (*Thermus thermophilus* and *Pyrococcus furiosus*) species[18,48,78–80]. Although small RNA silencing was not well studied in these organisms, these structures recapitulated expectations from metazoan research. Thus, their mammalian counterparts were presumed to be similar. However, it was many years until structures of full-length human Argonaute[19,20] and Dicer[81] were solved. In particular, human Dicer was analysed using cryo-EM, which has revolutionized the structural determination of larger proteins and complexes, while providing rich insights into dynamic states. We summarize recent insights into cryo-EM structures of human RNase III complexes during pri-miRNA/pre-miRNA cropping and dicing (Fig. 3).

Microprocessor cryo-EM studies

Initial biochemical[82] and structural[83] analyses utilized truncated Drosha (amino acids 390–1,365) with two copies of short DGCR8 carboxy-terminal peptides (amino acids 728–750), a minimal functional hetero-trimer that is active in microprocessing in vitro (Fig. 3a). In this model, Drosha alone recognizes the basal junctions and basal UG motif to determine cleavage sites ~11 bp from the basal pri-miRNA junction.

Although this minimal complex is active, the original structures did not fully explain microprocessing[83]. For example, the DGCR8 peptide used lacked the RNA-binding haem domain (RHED) and the dsRNA-binding domains (dsRBDs) (Fig. 3a), and thus does not account for DGCR8–pri-miRNA interactions. Moreover, DGCR8 can dimerize independently of Drosha via its haem-binding RHED domain, which enhances Microprocessor stability as well as pri-miRNA cleavage efficiency and fidelity[32,33,84,85]. Finally, the crystallized Drosha lacked the amino-terminal P-rich and RS-rich regions, whose functions are not fully understood at present (Fig. 3a).

Preparation of full-length recombinant Microprocessor is challenging owing to poor expression and aggregation of full-length proteins. However, cryo-EM enabled analysis of RNA-free, partially RNA-docked and fully RNA-docked structures, revealing dynamic interactions between Microprocessor and pri-miRNA[86,87] (Fig. 3b). For example, ~90° rotation of Drosha dsRBD during pri-miRNA loading enables extensive contacts with the pri-miRNA stem in a ravine between dsRBD and RNase IIIa/b domains (Fig. 3b). Moreover, one of the dsRBDs from DGCR8 and dsRBD of Drosha stack into a ruler that measures ~35 bp, providing a molecular basis for pri-miRNA length constraint. The low-resolution electron densities of the DGCR8 RHED domain appear to cap the apical loop[87], in line with biochemical data indicating that this region recognizes apical UGU motifs. However, the apical loop electron density lacked RNA in a substantial part of the path, and RHED dimers were not sufficiently resolved. The basal threshold of pri-miRNA is held in place by a four-way junction called the 'Buckle', comprising the Belt, Wedge, dsRBD and C-terminal region of Drosha (Fig. 3b). In addition to fastening the basal pri-miRNA in the fully docked state, the Belt domain acts as a conformational switch. In the RNA-free or partially docked states, the Belt domain occupies the RNA-binding cleft, a self-inhibited state of Microprocessor[86,87].

The atomic details revealed functionally essential residues and mechanisms for UG and mGHG motif recognition, providing a clear basis for their enrichment in high-throughput screens (Fig. 3a). Finally, these structures reveal insights into the molecular evolution of RNase III enzymes[86,87]. For example, the structural similarities of human Drosha to *Giardia* Dicer and human Dicer suggest common evolutionary origins, and features of RNA stem recognition and cleavage are even shared with bacterial RNase III[88].

Dicer cryo-EM studies

Dicer RNase III activity is central to miRNA biogenesis, RNAi and antiviral defence[89]. However, hidden layers of regulation are built into its structures and molecular interactions. Cryo-EM now

Table 1 | Recent technologies applied to the miRNA pathway

Methods	General attributes	Recent applications to the miRNA pathway
High-throughput substrate screening	Similar to classical in vitro selection assays Often involves parallel processing of a large endogenous substrate pool and/or library of designed or randomized variants Deep sequencing is used as a read-out, to infer functionally relevant features for processing	pri-miRNA features[30,31,36] pre-miRNA features[38,54]
Cryogenic electron microscopy (cryo-EM)	Uses an electron beam to image a specimen under cryogenic conditions Data are processed into electron microscopy densities that can be used to assign atomic coordinates Advantages include that cryo-EM is suitable for proteins or complexes of large molecular weight; relatively small amounts of sample are needed; multiple conformational states can be captured in a single experiment; and no need for crystallization	Mammalian Drosha/DGCR8 complex[86,87] Mammalian Dicer complexes[81,90,91] *Drosophila*Dicer complexes: Dicer-1 (ref. 92) and Dicer-2 (refs. 95,96) *Arabidopsis*Dicer complexes: DCL1 (ref. 93) and DCL3 (ref. 97)
Single-molecule assay	Offers real-time dynamics of biological reactions In vitro assays usually involve purified materials Observation times depend on the reaction kinetics, photostability and lifetime of fluorophores, but can go down to microseconds Detection is generally diffraction limited (~200–300 nm spatial resolution); however, single-molecule Förster resonance energy transfer (smFRET) operates at 1–10 nm, thus resolving intermolecular and intramolecular motions Single-molecule imaging in living cells is typically done with fluorescently tagged molecules and may utilize multimeric tags or scaffolds to enhance detection	Dynamic interplay of human Dicer and TRBP[94] In vitro target search and interrogation by human Ago2/RISC complexes[102–105,107] Live cell imaging of targeting and regulation by human Ago2 (refs. 108–110) Assembly and dynamics of *Drosophila* AGO2/RISC complexes[100,101]
RNA bind-n-seq (RBNS)	Yields relative quantitative binding affinities of an RNA-binding protein (RBP) across a library of target sites Typically, a purified RBP is incubated with a randomized pool of RNAs; co-purified RBP targets are then analysed by deep sequencing to identify their features	Ago2–miRNA complex binding affinity to target RNAs[64,65]
CRISPR–Cas9 screening	Genetic strategies for mutagenesis can be applied to identify factors involved in a cellular process of interest miRNA screening often incorporates a specific reporter as a functional read-out, enabling cell sorting before deep sequencing of enriched or depleted guide RNAs	ERH and SAFB2 in miRNA cluster assistance[153] ZSWIM8 in target-directed miRNA degradation (TDMD)[193,194]

Ago, Argonaute; miRNA, microRNA; pre-miRNA, precursor miRNA; pri-miRNA, primary miRNA; RISC, RNA-induced silencing complex; TRBP, transactivation responsive RNA-binding protein.

provides insights into how Dicer utilizes different cofactors, the enigmatic role of its helicase domain (Fig. 3c), selection mechanisms for different small RNAs and the structural basis for molecular ruler capacity.

Dicer cryo-EM studies from different organisms have recently expanded the rules of pre-miRNA and dsRNA dicing. These include human Dicer and its cofactor TRBP (transactivation responsive RNA-binding protein) bound to *pre-let*-7 (ref. 81), human Dicer in a dicing state bound to *pre-let-7a-1[GYM]* (ref. 90), mouse Dicer–TRBP bound to *pre-mir-15a* (ref. 91), *pre-let-7* processing by *Drosophila* Dicer-1–Loqs-PB complex[92] and the structures of *Arabidopsis* Dicer-like 1 (DCL1) with *pri/pre-mir-166f* (ref. 93). Overall, Dicer exhibits a hallmark L-shaped architecture (Fig. 3d). The DExD/H box helicase domain occupies the base, the RNase IIIa/b intramolecular dimer comprises the core and platform-PAZ domains form the cap. The initial cryo-EM structure of human Dicer exhibits a partially RNA-docked configuration where the helicase, dsRBD and PAZ helix lock it in a closed state[81]. Although human TRBP was reported to enhance substrate capture by Dicer[94], recent cryo-EM structures indicated that human Dicer can achieve the active dicing state without TRBP[90]. Transition from pre-dicing to active dicing states involves movement of the pre-miRNA stem into the catalytic centre, aided by conformational changes in the helicase-DUF283, dsRBD and PAZ helix domains. This is accompanied by sequence-independent electrostatic contacts between PAZ helix and RNA backbone, 5′-phosphate docking into the platform domain and interactions by dsRBD around the apical junction that include sequence-specific contacts favouring GYM motifs[90].

The mouse Dicer complexes are structurally similar to human Dicer, including a pre-catalytic state with partially docked pre-miRNA and a catalytic state with fully docked RNA and disordered N-terminal helicase-DUF283 domains[91]. However, unlike the human studies, mouse TRBP was shown to promote the catalytic state of Dicer (13% of particles). Importantly, a mouse Dicer mutant lacking the Hel1 subdomain had enhanced, aberrant capacity to fully dock pre-miRNAs with long stems and larger loops (including a subset of mirtrons), resulting in enhanced accumulation of these small RNAs in vivo and animal lethality[91]. Therefore, partially docked structures may represent a kinetic checkpoint selecting genuine pre-miRNAs from the slew of cellular RNA hairpins and dsRNAs (Fig. 3d).

In contrast to mammalian Dicers, the miRNA processing fly Dicer-1 acquired a catalytic structure by belting the pre-miRNA backbone with Dicer-1 dsRBD and Loqs-PB dsRBD2 (ref. 92). In plants, DCL1 structural studies highlight the unique and conserved structure–function features of Dicer across distant eukaryotes[93]. Finally, additional contemporary studies report an array of structures for active short interfering RNA (siRNA) processing by *Drosophila* Dicer-2/R2D2 (ref. 95) or Dicer-2/Loqs-PD (ref. 96) and *Arabidopsis* Dicer-like 3 (DCL3)[97]. Collectively, these studies reveal similar domain arrangements to miRNA processing Dicers, while showing dynamic structural strategies in regulated siRNA production.

Single-molecule imaging of miRNA factors

Despite providing atomic-level information, cryo-EM and X-ray crystallography yield static snapshots that only indirectly inform molecular dynamics. A complementary approach involves real-time single-molecule imaging, which can directly visualize conformational changes, molecular heterogeneities and transient intermediates otherwise lost in ensemble averaging. Building on the strong history of small RNA biochemistry, in vitro single-molecule imaging has recently gained traction in the small RNA field. Efforts include confirming the heterotrimeric structure of Microprocessor[82,83,98], coordinated activities of human Dicer and TRBP[94], dsRNA processing by fly Dicer-2/Loqs-PD[99], assembly and maturation of Ago/RISC[100–102], and finally, target interrogation and gene silencing by Ago/RISC[103–110].

Human Dicer and TRBP single-molecule imaging studies revealed a rapid and dynamic selection of pre-miRNAs from a sea of other hairpins, which depends on proper 3′ docking into the PAZ domain[94]. In *Drosophila* Dicer-2/Loqs-PD studies, dsRNA translocation, RNA cleavage and dynamic selection of different termini were visualized in real time[99]. These examples demonstrate the capacity of single-molecule imaging to dissect and resolve highly dynamic processes, which are not amenable to biochemical, genetics or structural studies.

Although Argonaute proteins have been extensively scrutinized using X-ray crystallography[111,112], single-molecule imaging has been particularly useful to elucidate dynamic Ago maturation and function. For example, imaging of dynamic assembly of fly RISC complexes showed that Hsp70/90 chaperones activate RISC by stabilizing open Ago2 confirmation[100,101]. Single-molecule Förster resonance energy transfer (smFRET) experiments extended these studies by directly imaging internal structural motions within human Ago[102,106] (Fig. 3e). The Ago2 structural element Helix-7 divides seed pairing by introducing a kink near the 3′ end of the seed (nucleotides 6–8), which interrupts the pre-formed α-helical arrangement of the 5′ seed region. Helix-7 moves away upon productive seed pairing, and this dynamic reshaping of seed pairing enables Ago to reject inappropriate target sites[106]. smFRET also visualizes continuously dynamic interactions of the Ago-PAZ domain with the miRNA 3′ end within ternary Ago–miRNA–target complexes of various pairing configurations[102]. Such 3′ dynamics seem particularly relevant to expose the miRNA 3′ end in the presence of 3′ supplementary base-pairing[102,113] (which triggers Ago degradation, as discussed in 'Regulation of miRNA turnover').

Fluorescence co-localization and smFRET experiments also provide insights into target searching by Ago/RISC. For example, kinetic and thermodynamic parameters suggest Ago functions by modifying the free energy landscape of RNA hybridization[103]. Additional smFRET studies using tandem target sites demonstrated repetitive shuttling of a single human Ago2/RISC by 1D facilitated diffusion, enabling rapid target interrogation compared with the 3D collision between targets and the RISC[105]. Finally, going beyond in vitro reactions, in vivo single-molecule imaging can visualize the dynamic interplay between mRNA translation and gene silencing by Ago/RISC complexes in living cells[108–110]. Such studies demonstrate that translation facilitates access of Ago2 to mediate target cleavage within coding regions, and that target site exposure limits the rate of mRNA cleavage by RISC.

Overall, single-molecule imaging shines a light on the highly dynamic and multi-step nature of miRNA processing and regulation.

Regulation of miRNA biogenesis

Typical biogenesis schematics imply an unfettered route to generate miRNAs (Fig. 1). Yet miRNA production is not constitutive but, instead, tightly regulated at multiple levels. These can promote or inhibit miRNA production, and can occur at various steps of miRNA biogenesis. Investigation of this topic has benefited from multiple approaches, including detailed analysis of individual miRNA substrates and factors, as well as large-scale genomics and CRISPR screening (Table 1).

One of the first cases of regulated miRNA biogenesis regards the control of let-7 family maturation by Lin28 RBPs[114–117] (Fig. 4a). These recognize a conserved loop motif in *pre-let-7* and recruit terminal uridyltransferases (TUTases) TUT4/7 to oligouridylate *pre-let-7* (refs. 118,119), which triggers its degradation via Dis3L2 (refs. 120–122). Amongst the large family of mammalian let-7 miRNA loci, those that are inhibited by Lin28/TUTase/Dis3L2 are classified as Group I members. Other let-7 members bear suboptimal one-nucleotide 3′ pre-miRNA overhang following Microprocessor cleavage, rendering them poor Dicer substrates (Group II). But in the absence of Lin28, such *pre-let-7* hairpins can be monouridylated by TUT4/7 to restore a two-nucleotide overhang that enhances Dicer processing[123]. 3′ tailing of pre-miRNA can also adjust the site of Dicer cleavage, thereby either changing the miRNA seed sequence or even switching which miRNA duplex arm is the dominant functional product[124].

The biogenesis of other miRNA precursors is likely to be regulated, as summarized in recent comprehensive reviews[125,126]. Presumably, the catalogue of miRNA biogenesis regulation will continue to expand, based on several observations. These include that numerous miRNA loci bear conserved loop sequences of unknown functions, but imply regulation[127]; large-scale CLIP analyses reveal numerous RBP interactions with specific miRNA precursors[128]; and in vitro pull-down assays of pre-miRNAs with cell lysates also recover many specific RBP and miRNA interactions[129]. Here, we highlight some recent concepts in regulated miRNA biogenesis.

Cross-regulation and homeostatic control of miRNA pathway factors

miRNA pathway autoregulation has repeatedly been uncovered in diverse settings. For example, auto-targeting of Dicer by miRNAs is relevant in certain cancers[130,131], and other miRNA factors are preferentially targeted by miRNAs[132]. Another layer of regulation involves control of Ago proteins by miRNA availability, as unloaded Ago proteins are subject to degradation by ubiquitination or autophagy[133–136].

A prominent example involves the reciprocal cross-regulation of Drosha and DGCR8 (Fig. 4b). The 5′ UTR and CDS regions of mammalian *Dgcr8* bear hairpins (*mir-3618* and *mir-1306*) that are cleaved by Drosha, thereby suppressing DGCR8 (ref. 137). By contrast, DGCR8 stabilizes and solubilizes Drosha through protein–protein interactions. This cross-regulation between Drosha and DGCR8 enables homeostatic control of Microprocessor activity and is conserved in different animal species[137–139].

Although the *Dgcr8* hairpins are annotated as miRNAs, they do not yield substantial levels of mature miRNA, partly due to nuclear accumulation of the hairpins[137]. Thus, their main known role is in *cis*-regulation. Recently, the biological impact of Microprocessor cross-regulation was investigated[140]. During differentiation of mouse embryonic stem cells, an alternative transcription start site downstream of the first *Dgcr8* hairpin yields an isoform that evades Microprocessor autoregulation and leads to the accumulation of DGCR8 protein. The imbalanced DGCR8:Drosha protein stoichiometry and non-functional Microprocessor aggregation reduced nuclear miRNA biogenesis with an impact on miRNA-mediated repression and embryonic development[140].

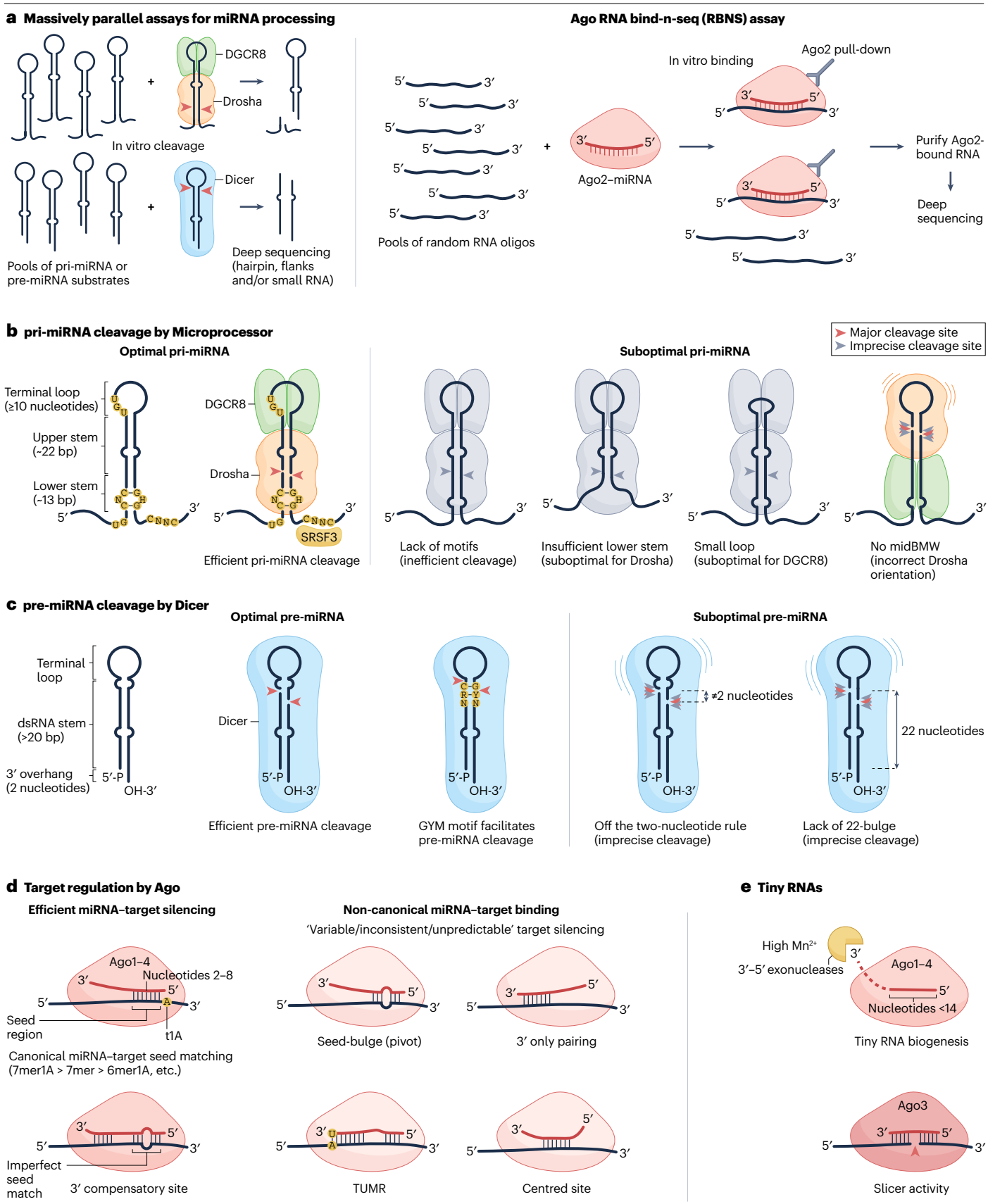
a Massively parallel assays for miRNA processing
DGCR8
Drosha
In vitro cleavage
Dicer
Pools of pri-miRNA or pre-miRNA substrates
Deep sequencing (hairpin, flanks and/or small RNA)
Ago RNA bind-n-seq (RBNS) assay
Pools of random RNA oligos
Ago2–miRNA
In vitro binding
Ago2 pull-down
Purify Ago2-bound RNA
Deep sequencing
b pri-miRNA cleavage by Microprocessor
Major cleavage site
Imprecise cleavage site
Optimal pri-miRNA
Terminal loop (≥10 nucleotides)
Upper stem (~22 bp)
Lower stem (~13 bp)
DGCR8
Drosha
SRSF3
Efficient pri-miRNA cleavage
Suboptimal pri-miRNA
Lack of motifs (inefficient cleavage)
Insufficient lower stem (suboptimal for Drosha)
Small loop (suboptimal for DGCR8)
No midBMW (incorrect Drosha orientation)
c pre-miRNA cleavage by Dicer
Terminal loop
dsRNA stem (>20 bp)
3′ overhang (2 nucleotides)
5′-P
OH-3′
Optimal pre-miRNA
Dicer
Efficient pre-miRNA cleavage
GYM motif facilitates pre-miRNA cleavage
Suboptimal pre-miRNA
≠2 nucleotides
Off the two-nucleotide rule (imprecise cleavage)
22 nucleotides
Lack of 22-bulge (imprecise cleavage)
d Target regulation by Ago
Efficient miRNA–target silencing
Ago1–4
Nucleotides 2–8
Seed region
t1A
Canonical miRNA–target seed matching (7mer1A > 7mer > 6mer1A, etc.)
Imperfect seed match
3′ compensatory site
Non-canonical miRNA–target binding
'Variable/inconsistent/unpredictable' target silencing
Seed-bulge (pivot)
3′ only pairing
TUMR
Centred site
e Tiny RNAs
High Mn2+
3′–5′ exonucleases
Ago1–4
Nucleotides <14
Tiny RNA biogenesis
Ago3
Slicer activity

Fig. 2 | Structural and sequence features of miRNA substrates and targets. **a**, Design of massively parallel assays and RNA bind-n-seq (RBNS) assays for identifying microRNA (miRNA) pathway substrates and targets. Left: a library of primary miRNA (pri-miRNA) or precursor miRNA (pre-miRNA) substrates is incubated with purified Microprocessor (upper) or Dicer complex (lower) for in vitro cleavage, or for in vivo processing in cells. The reaction products are analysed by deep sequencing to infer structural features and sequence motifs within effective substrates. Right: target RNA oligo pools with random sequences are incubated with purified Ago2 loaded with a specific miRNA. Sequencing of bound species permits the relative affinities of different target sequences to be inferred. **b**, pri-miRNA features. An optimal pri-miRNA contains characteristic structural features (single-stranded flanking regions, a ~35 bp double-stranded RNA (dsRNA) stem and an apical loop ≥10 nucleotides), primary motifs (including UG in the basal junction, UGU/GUG in the apical junction and CNNC in the 3′ flanking region) and chimeric structure-motif features such as the mismatched GHG (mGHG) in the lower stem. Drosha recognizes the basal junction, UG motif and mGHG, and measures ~11 bp from the basal junction to cleave the dsRNA stem (red arrowheads). The DGCR8 dimer recognizes the apical loop and the UGU/GUG motif. Accessory factors can regulate microprocessing of pri-miRNA, including binding of CNNC by SRSF3. pri-miRNAs with suboptimal features such as missing motifs, an unpaired lower stem and/or small apical loop exhibit inefficient and/or imprecise cleavage. Note that a middle bulge, mismatch and wobble base pair (midBMW) in the upper stem can repress unproductive cleavage by Microprocessor from the apical loop side. **c**, pre-miRNA features. An optimal pre-miRNA hairpin contains 5′-monophosphate, a two-nucleotide 3′-end overhang, a double-stranded stem of >20 bp and a single-stranded terminal loop. Dicer can measure its cleavage site from both 5′ and 3′ hairpin ends, although not all pre-miRNA substrates are engaged at both termini. A GYM (paired G, paired pyrimidine and mismatched C or A) motif near the Dicer cleavage site promotes pre-miRNA processing. A bulge/mismatch near the dicing sites enhances Dicer cleavage efficiency and/or accuracy, when the first nucleotide of the miRNA-3p species is two nucleotides from the bulge/mismatch or when there is a 22-nucleotide bulge in the pre-miRNA 3′ arm. Lack of this feature can cause Dicer to cut poorly and/or imprecisely, yielding multiple miRNA isoforms or lower small RNA levels. **d**, Argonaute (Ago)–miRNA interaction features. Left, top: the canonical miRNA–target interaction is mediated by seed pairing between nucleotides 2 and 8 (seed region) of miRNA with target RNA, and is often sufficient for measurable target repression. Shorter seed regions can also be functional, especially when followed by an adenosine opposite the first miRNA position (t1A). 7mer1A, seed 2–8 pairing with t1A; 7mer, seed 2–8 pairing; 6mer1A, seed 2–7 with t1A. Left, bottom: a special class of target interaction with discontinuous seed pairing is compensated by extensive 3′ pairing. Right: various miRNA–target interactions lacking canonical seed pairing are found from in vivo Ago2-CLIP assays, in vitro Ago2-RBNS data and bioinformatics; four types are summarized here. In general, the efficacy of these non-canonical sites is weak or controversial, and they were mostly assayed in vitro or in reporter systems. Unlike the exemplary 3′ compensatory let-7 site in *lin-41*, whose non-seed pairing is critical for *Caenorhabditis elegans* development, the impact of other non-canonical sites is mostly unknown. **e**, Tiny RNAs. Under in vitro conditions of high manganese, several 3′–5′ exoribonucleases (ISG20, TREX1 and ERI1) can trim Ago-loaded miRNA down to <14 nucleotides, and ISG20-mediated trimmed miRNA activates Ago3 cleavage of target mRNA. TUMR, tail-U-mediated repression.

Regulation of suboptimal miRNAs in genomic clusters

Although most miRNAs are transcribed as single loci, approximately one third of vertebrate miRNAs reside in genomic clusters, where two or more miRNA hairpins are cleaved from the same primary transcript. The reasons for miRNA clustering are not fully known, but it is presumed to facilitate miRNA co-expression[141]. miRNA loci from clusters are usually functional when expressed experimentally as solo constructs. However, cases of miRNA cluster regulation exist, including the *mir-17-92* cluster which exhibits stepwise cleavage of different cluster members[142,143]. Additional studies across different species, and even viruses, reveal that biogenesis of specific miRNAs depends on cluster location[144–147].

Recent studies reveal that microprocessing of suboptimal mammalian miRNA hairpins is enhanced by an optimal miRNA neighbour (Fig. 4c). An archetype for this is *mir-451*, whose short stem and small terminal loop are integral to its unusual Dicer-independent, Ago2-dependent, biogenesis strategy[148] (Fig. 1c). Although these features render it an extremely suboptimal Microprocessor substrate, miR-451 is nonetheless a highly abundant erythroid miRNA[149,150] whose nuclear processing is strongly enhanced by proximity to its operon neighbour *mir-144* (refs. 151,152). Mechanistically, following efficient recruitment and cleavage of *pri-mir-144* by Microprocessor, the released complex is in proximity to cleave nearby *pri-mir-451* (refs. 151,152). The identity and relative location of the neighbouring miRNA is not critical for this, and maturation of the neighbouring miRNA can be uncoupled from enhancement of *pri-mir-451* cleavage. In particular, substituting the miRNA neighbour with synthetic sites that directly recruit DGCR8 can still enhance miR-451 biogenesis[151].

Parallel work on the *mir-15a/16* cluster utilized CRISPR–Cas9 screening to identify factors that are selectively required for suboptimal miR-15a. A dual genetic screen was conducted using cells that harbour GFP and RFP transgenes whose 3′ UTRs bear multiple sites for miR-15a and miR-16, respectively[153]. In this background, CRISPR–Cas9 hits that selectively derepress the reporter for suboptimal miR-15a, while maintaining repression of the miR-16 reporter, comprise candidates for miRNA neighbour enhancement. Amongst several such hits, SAFB1/2 and ERH were confirmed as positive factors in the processing of suboptimal miRNAs[152,153].

A pressing question regards the molecular mechanisms by which these factors promote Microprocessor activity. ERH binds DGCR8 directly, and ERH dimerization may assist DGCR8 dimerization within Microprocessor[154]. A specific domain of SAFB2 interacts with the N-terminal region of Drosha and is sufficient to recapitulate cluster assistance[153]; however, another study found that the N-terminal region of Drosha is dispensable for cluster assistance[152]. The discrepancy remains to be resolved. At present, several models seem compatible with the available data (Fig. 4c). In one scenario, after recruitment and release of Microprocessor from the optimal hairpin, Microprocessor can identify the suboptimal hairpin, but its interaction is unstable. In that model, ERH and SAFB1/2 may help stabilize the complex and activate cleavage of the suboptimal miRNA hairpin. Alternatively, ERH and SAFB1/2 might facilitate dimerization of Microprocessor units to promote processing of suboptimal miRNA hairpins.

Curiously, although *mir-144* knockout in K562 human lymphoblast cells illustrates a strong reliance of *mir-451* biogenesis on its canonical partner[151,152], maturation of miR-451 is only subtly affected in zebrafish *mir-144* knockouts[150], suggesting that other strategies can enhance nuclear processing of *mir-451*. Although these remain to be elucidated, it is worth noting that nuclear processing of miRNAs is co-transcriptional[155–157], and transcription and chromatin retention can affect Microprocessor activity on pri-miRNA transcripts[158–160]. Their impact on suboptimal miRNAs deserves further investigation.

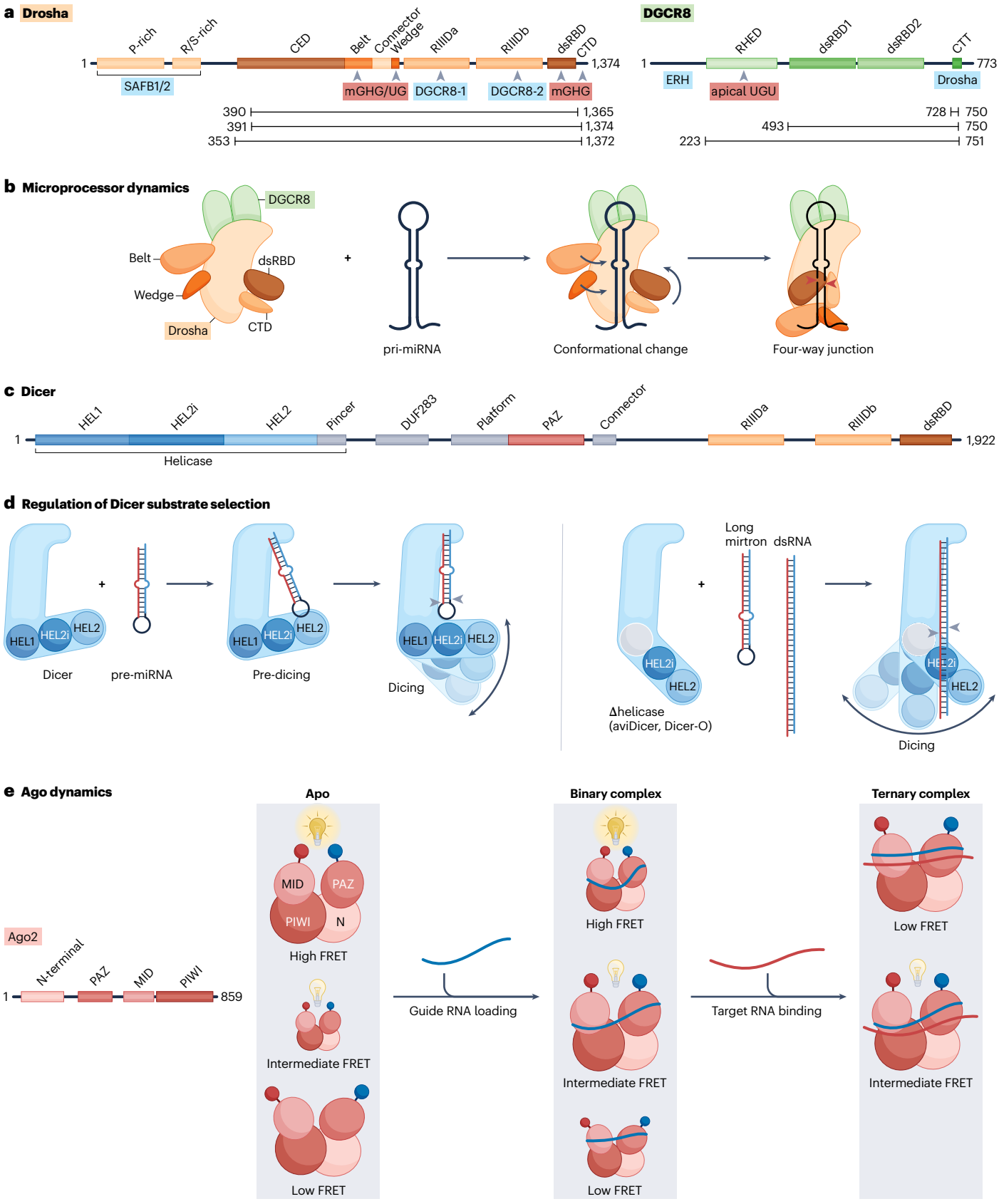
a Drosha
P-rich
R/S-rich
CED
Belt
Connector
Wedge
RIIIDa
RIIIDb
dsRBD
CTD
1
1,374
SAFB1/2
mGHG/UG
DGCR8-1
DGCR8-2
mGHG
390
1,365
391
1,374
353
1,372
DGCR8
RHED
dsRBD1
dsRBD2
CTT
1
773
ERH
apical UGU
Drosha
728
750
493
750
223
751
b Microprocessor dynamics
DGCR8
Belt
dsRBD
Wedge
Drosha
CTD
+
pri-miRNA
Conformational change
Four-way junction
c Dicer
HEL1
HEL2i
HEL2
Pincer
DUF283
Platform
PAZ
Connector
RIIIDa
RIIIDb
dsRBD
1
1,922
Helicase
d Regulation of Dicer substrate selection
HEL1
HEL2i
HEL2
Dicer
+
pre-miRNA
Pre-dicing
Dicing
Long
mirtron
dsRNA
Δhelicase
(aviDicer, Dicer-O)
Dicing
e Ago dynamics
Ago2
N-terminal
PAZ
MID
PIWI
1
859
Apo
MID
PAZ
PIWI
N
High FRET
Intermediate FRET
Low FRET
Guide RNA loading
Binary complex
High FRET
Intermediate FRET
Low FRET
Target RNA binding
Ternary complex
Low FRET
Intermediate FRET

Fig. 3 | Cryo-EM and single-molecule studies of Microprocessor and Dicer complexes. a, Linear domain arrangements of Drosha and DGCR8. The portions that bind other protein factors (blue) or recognize specific miRNA motifs (red) are indicated. The different Drosha and DGCR8 truncations used in different structural studies are indicated (amino acids 390–1,365 (ref. 83), 391–1,374 (ref. 86) and 353–1,372 (ref. 87)). **b**, Structural rearrangements of Microprocessor upon transitioning from Apo state to a partially docked primary microRNA (pri-miRNA) in the catalytic state. **c**, Linear domain arrangement of Dicer. **d**, Dicer regulation via the amino-terminal helicase domain. In mammals, full-length Dicer adopts an L-shape structure and recognizes the 5′ and 3′ termini of precursor miRNAs (pre-miRNAs). Left: the helicase domain can flexibly interact with the terminal loop region in a pre-dicing state, but when it shifts position the pre-miRNA can move and align with the main body of Dicer and access the catalytic sites. Due to the overall compact L-shape structure of Dicer during the whole process, only shorter pre-miRNA substrates are efficiently bound and cut by Dicer. Right: upon experimental deletion of the helicase domain, or in natural isoforms that remove parts of this region (such as aviDicer and Dicer-O), the Dicer N terminus remains flexible and does not form a compact L-shape structure. This permits additional substrates to access Dicer for cleavage into small RNAs (such as double-stranded RNA (dsRNA) and certain long mirtron hairpins). **e**, Single-molecule Förster resonance energy transfer (smFRET) visualizes internal structural changes of human Ago2 during target interrogation. Left: Ago2 domains. Right: smFRET assays. A FRET donor (blue) and an acceptor (red) are incorporated site-specifically into PAZ and MID domains. The energy transfer efficiency (denoted by the brightness of the light bulb above the structures) between the two dyes reports on the physical separation between the two domains, hence the conformational state of Ago2. Three major conformational states of apo Ago2 are indicated by three FRET states, where the protein size corresponds to the relative frequency of each state. Guide strand loading changes the frequencies of conformational states, with only slight changes in their FRET values. However, base-pairing with a target reduces the conformational flexibility of Ago2 to only two compact states. Ago, Argonaute; cryo-EM, cryogenic electron microscopy; CTD, carboxy-terminal domain; dsRBD, double-stranded RNA-binding domain; mGHG, mismatched GHG; RHED, RNA-binding haem domain.

Regulation of Dicer activity via its N terminus/helicase domain

Dicer was initially isolated via cleavage activity on long dsRNA substrates[161], and subsequently realized to process pre-miRNA hairpins[162]. Plants and arthropods encode multiple Dicers, which have distinct preferences for miRNAs and dsRNAs. Although mammals harbour only one Dicer gene, its isoforms exhibit functional diversity. For example, an intronic promoter derived from a rodent-specific retrotransposon insertion yields Dicer-O, an N-terminally truncated Dicer isoform expressed specifically in oocytes[163]. This isoform lacks part of its helix domain and has enhanced activity to process long dsRNA into endogenous siRNAs. Indeed, mouse oocytes are a unique mammalian setting where siRNAs are not only abundant and functional[164,165] but may play a dominant regulatory role instead of miRNAs or piwi-interacting RNAs[166–168]. However, as the canonical Dicer isoform is prevented from processing long dsRNA through its N-terminal helix domain, this raises questions as to its involvement in antiviral defence, especially as long dsRNA activates the interferon pathway as a dominant antiviral response[169].

Interestingly, experimental deletion of the Dicer N terminus enhances its capacity to cleave viral dsRNA during infection[170]. Recently, an endogenous N-terminally truncated Dicer isoform (aviDicer) lacking the helix domain was identified[171]. aviDicer is generated by alternative splicing and is apparently of low abundance; nevertheless, it is detected in certain stem cells, proposed as settings of antiviral activity by mammalian RNAi[172,173]. Loss of the helicase domain unlocks Dicer and expands its processing capacity on substrates bearing extended dsRNA stems[91] (Fig. 3d). Thus, there may be cell-specific requirements to regulate substrate selection by mammalian Dicer, for endogenous regulatory purposes or to enable restriction of foreign nucleic acids.

Regulation of miRNA turnover

The lifetime of different RNA molecules varies tremendously, and the same RNA can have distinct dynamics in different settings or conditions. Such observations indicate distinct regulatory pathways for RNA decay. However, for many years this was not thought to be a substantial route for miRNA regulation, as most miRNAs seemed extremely stable. For example, whereas the average mRNA half-life is 2–4 h (with some decayed within minutes), the half-life of many miRNAs is days[174] to weeks[175,176]. The stability of mature miRNAs is attributed to their tight association with Ago proteins, which protects them from exoribonucleases. Eventual dissociation of the Ago–miRNA complex results in turnover of unloaded Ago[133,135,177] via the Iruka E3 ubiquitin ligase[134], along with exoribonucleolytic degradation of free miRNAs (Fig. 5a).

Introduction of nucleoside analogues into cells enables temporally resolved characterization of transcript dynamics. This approach validated the general stability of mature miRNAs and rapid degradation of their duplex partner passenger strands, which are not retained in Ago/RISC[176,178]. However, these studies also reveal substantial variation in the stability of mature miRNAs, implying strategies for their regulated turnover. In addition, analysis of in vivo settings revealed differences from cultured cells, such as that miRNA turnover is accelerated in neurons[179]. Several nucleases were indeed reported to degrade miRNAs in different organisms[180–184], although the mechanisms that underlie their specificity and action are often not well understood. Moreover, a dozen years ago, the viral transcripts *HSUR1* and m169 were found to specifically degrade cognate miRNAs with extensive complementarity[185,186]. Later, it was shown that mRNA can also serve as triggers for miRNA degradation[187]. This process became known as target-directed miRNA degradation (TDMD) and was demonstrated to compete with miRNA-directed decay of the mRNA target[188].

miRNA tailing

Early studies indicated that engagement of miRNA with a highly complementary target can induce miRNA tailing or trimming[188,189]. As mentioned above, literature on the inhibitory consequences of tailing and trimming on pre-miRNA, along with studies that connected 3′ untemplated modifications with miRNA dynamics[70,190], led to the notion that tailing and trimming processes underlie TDMD. However, careful molecular genetic studies indicate that 3′ untemplated modifications constitute a parallel regulatory pathway largely separate from miRNA decay[176]. This conclusion was echoed with the analysis of cells that coordinately delete the major known miRNA tailing enzymes (TENT2, TUT4 and TUT7) as well as Dis3L2 (refs. 191,192), in which TDMD triggers retain capacity for miRNA downregulation. Thus, other regulatory mechanisms for TDMD must exist.

TDMD: ZSWIM8 mediates ubiquitination of Ago2 engaged with highly complementary target

Two recent studies used CRISPR screening to elucidate the mechanism of TDMD[193,194]. Both studies exploited the endogenous TDMD trigger — the non-coding RNA *Cyrano* — which is highly complementary and

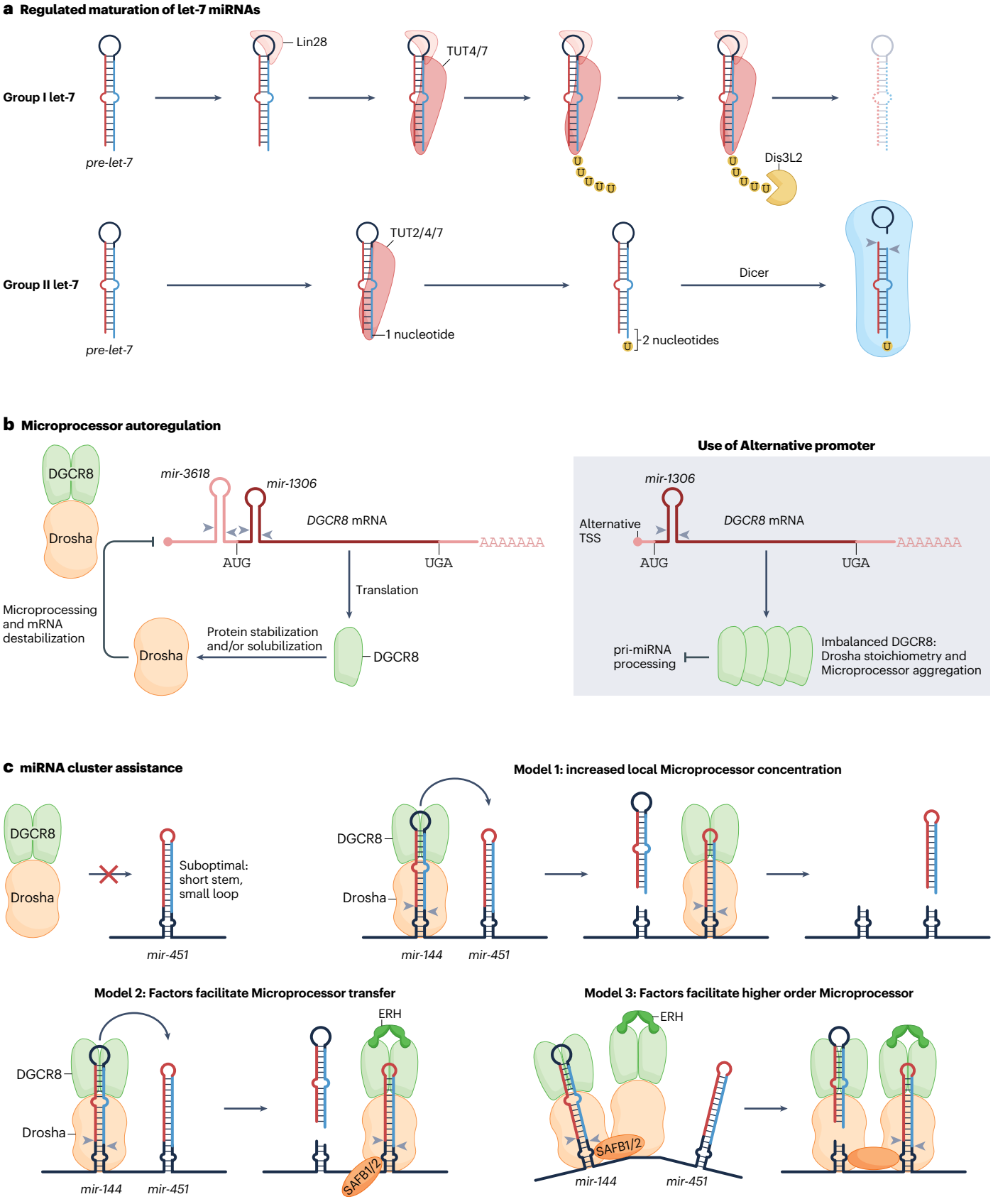
a Regulated maturation of let-7 miRNAs
Group I let-7
pre-let-7
Lin28
TUT4/7
Dis3L2
Group II let-7
pre-let-7
TUT2/4/7
1 nucleotide
2 nucleotides
Dicer
b Microprocessor autoregulation
DGCR8
Drosha
mir-3618
mir-1306
DGCR8 mRNA
AUG
UGA
AAAAAAA
Translation
Microprocessing and mRNA destabilization
Drosha
Protein stabilization and/or solubilization
DGCR8
Use of Alternative promoter
mir-1306
Alternative TSS
DGCR8 mRNA
AUG
UGA
AAAAAAA
pri-miRNA processing
Imbalanced DGCR8: Drosha stoichiometry and Microprocessor aggregation
c miRNA cluster assistance
DGCR8
Drosha
Suboptimal: short stem, small loop
mir-451
Model 1: increased local Microprocessor concentration
DGCR8
Drosha
mir-144
mir-451
Model 2: Factors facilitate Microprocessor transfer
DGCR8
Drosha
mir-144
mir-451
ERH
SAFB1/2
Model 3: Factors facilitate higher order Microprocessor
ERH
SAFB1/2
mir-144
mir-451

Fig. 4 | Strategies for the regulation of miRNA biogenesis. a, Two strategies of regulated maturation of let-7 microRNAs (miRNAs) by 3′ tailing. With group I loci, Lin28 binds the terminal loop of *pre-let-7* and recruits terminal uridyltransferases (TUTases) TUT4/7 to oligouridylate its 3′ end, which triggers its degradation via Dis3L2. With group II loci, the initial Drosha-cleaved *pre-let-7* only has a one-nucleotide 3′ overhang, rendering it a suboptimal Dicer substrate. However, this defect can be rescued by 3′-monouridylation via TUT2/4/7 to yield a two-nucleotide overhang, especially in the absence of Lin28. **b**, Autoregulation of Microprocessor. Left: the *DGCR8* mRNA bears two hairpins within its 5′ untranslated region (UTR) and coding sequence (CDS) (*mir-3618* and *mir-1306*), which can be cleaved by Drosha (arrowheads). This destabilizes *DGCR8* transcripts and reduces protein production. Reciprocally, DGCR8 protein positively regulates Microprocessor by stabilizing or solubilizing Drosha protein. Right: during differentiation of mouse embryonic stem cells, however, usage of an internal promoter yields a shorter *DGCR8* isoform lacking *mir-3618*, which escapes Microprocessor autoregulation. The resulting accumulation of DGCR8 imbalances DGCR8:Drosha protein stoichiometry, resulting in Microprocessor aggregation and reduced primary miRNA (pri-miRNA) processing. **c**, Enhanced biogenesis of suboptimal miRNAs within a genomic cluster. Certain miRNAs that lack optimal Microprocessor features (such as Dicer-independent *mir-451*) are poorly processed by themselves but are rescued by a neighbouring optimal miRNA (such as the normal context of *mir-144/451* operon). Several models remain in play to explain this process, including increased local availability of Microprocessor via the miRNA helper, and various roles involving auxiliary RNA-binding proteins (RBPs) such as ERH and SAFB1/2. These might stabilize Microprocessor on a suboptimal hairpin or bridge Microprocessor complexes via dimerization.

abundantly bound to *miR-7* (refs. 195,196). *Cyrano* mutants strongly upregulate *miR-7* (ref. 197), setting the stage for genetic screens for other mutants that similarly upregulate *miR-7*, recovered via decreased fluorescence from a GFP-*miR-7* sensor. Surprisingly, such screens reveal that factors involved in protein turnover, rather than RNA turnover, mediate TDMD[193,194]. A central factor is ZSWIM8, which binds Ago2 and recruits a multiprotein ElonginB–C-Cul3 ubiquitin ligase complex to tag Ago2 protein for proteasome-mediated turnover (Fig. 5b).

A protein-based mechanism for selective miRNA turnover was unexpected but is, in retrospect, an appealing strategy. Pairing to the TDMD target releases the miRNA 3′ end, accompanied by structural rearrangement of Ago[113] (Fig. 5b). Selective decay of Ago2, which requires surface-exposed lysines[193,194], would release the free miRNA for degradation. A future challenge will be to elucidate how ZSWIM8 selectively recognizes the form of Ago2 engaged in TDMD. In addition, a new study concluded that TDMD in *C. elegans* does not necessarily require 3′ end pairing[198]. Thus, additional mechanistic surprises for TDMD may await.

The elucidation of TDMD paves the way for understanding its biological impact. TDMD requires extensive base-pairing between target RNA and miRNA sequences in the seed region and 3′ end, but not the central region. This knowledge can be used to prioritize TDMD candidates through bioinformatics or experimental approaches such as Ago-CLASH, where miRNAs are directly ligated to targets[199]. More importantly, the discovery of the TDMD-specific factor ZSWIM8 opens a more direct path into TDMD networks, as *zswim8* mutants across a broad range of species upregulate select cohorts of miRNAs[193]. Such data pinpoint miRNAs with greatest suppression via TDMD and provide a gauge for the functional efficacy of individual TDMD targets.

Although the field is young, several studies have identified endogenous TDMD triggers whose miRNA binding sites induce substantial miRNA degradation. In mouse brain, knockout of the long non-coding RNA and TDMD trigger *Cyrano*, or even specific knockout of the *Cyrano* miR-7 binding site, induces miR-7 levels 40-fold to 50-fold (ref. 197). However, *Cyrano* knockout mice have only subtly increased repression of miR-7 targets and appear phenotypically normal. Disrupting the TDMD site of *miR-29b* in the 3′ UTR of mouse *NREP* increases *miR-29b* levels and impairs coordination and motor learning[200]. Finally, in *D. melanogaster*, multiple functional TDMD targets were validated, for which mutation of endogenous highly complementary target sites upregulates the cognate miRNAs[201,202]. Notably, disruption of a TDMD trigger (the long non-coding RNA *Marge*) for *miR-310* family miRNAs results in defective embryonic cuticle formation[201,202]. Moreover, the miRNA effector AGO1 contains a TDMD trigger for miR-999, and its mutation in flies upregulates miR-999 and impairs stress tolerance[202]. These in vivo genetic tests demonstrate regulatory and biological significance of individual TDMD triggers.

Although ZSWIM8 clearly mediates TDMD restriction of miRNA accumulation, this is not to say that tailing or trimming does not impact cellular miRNA pools. For example, 3′-adenylation can stabilize certain miRNAs[203,204], but has also been suggested to induce miRNA degradation[181]. Recently, it was reported that mutation of the miRNA deadenylase USB1 in the disease poikiloderma with neutropenia leads to miRNA downregulation and derepression of miRNA targets[205]. Overall, as discussed with miRNA uridylation, the impact of miRNA adenylation on their in vivo accumulation is not straightforward to predict, and may not necessarily affect levels[206]. Further study of the functional impacts of tailing enzymes are needed for a comprehensive understanding of their positive and negative roles in shaping miRNA pools[207,208].

Conclusions and future challenges

The application of new techniques to the miRNA field continues to yield fundamental insights into the operation of core miRNA factors and substrates, as well as new layers of regulated miRNA processing and function. For most of the experimental strategies discussed, there are clear next steps to follow. For example, only a few miRNAs were assessed in structural studies of miRNA biogenesis factors (Fig. 3a–d). As endogenous miRNAs vary widely in their biogenesis efficiency (Fig. 2a–c), including diverse miRNAs in future cryo-EM studies will be informative for both Microprocessor and Dicer substrates. This may yield insights into how Microprocessor cofactors such as ERH and SAFB contribute to the biogenesis of suboptimal and/or clustered miRNAs (Fig. 4c).

Single-molecule imaging uniquely provides direct visualization of dynamic miRNA processing and regulatory complexes. However, it is notable that in vitro studies of Microprocessor have been notably lacking (compared with Dicer and Ago), whereas in vivo assays have mostly focused on Ago (Fig. 3e) with little application to miRNA biogenesis factors thus far. In particular, the subcellular contexts of Microprocessor[156–160] and Dicer[209,210] are functionally relevant and should be explored further in the future.

As mentioned, miRNA biogenesis is often not a straight shot from primary transcript to mature small RNA (Fig. 1) but can be highly regulated (Fig. 4). There is surely much more to learn, given the existence of numerous phylogenetically conserved miRNA hairpin loops[127] and extensive catalogues of specific associations between RBPs and miRNA precursors[128,129], which generally remain to be studied. For instance, recent work shows that *mir-144*, the canonical partner of Dicer-independent *mir-451*, is itself highly regulated. This involves structural rearrangement of the *pre-mir-144* stem into a Dicer-competent

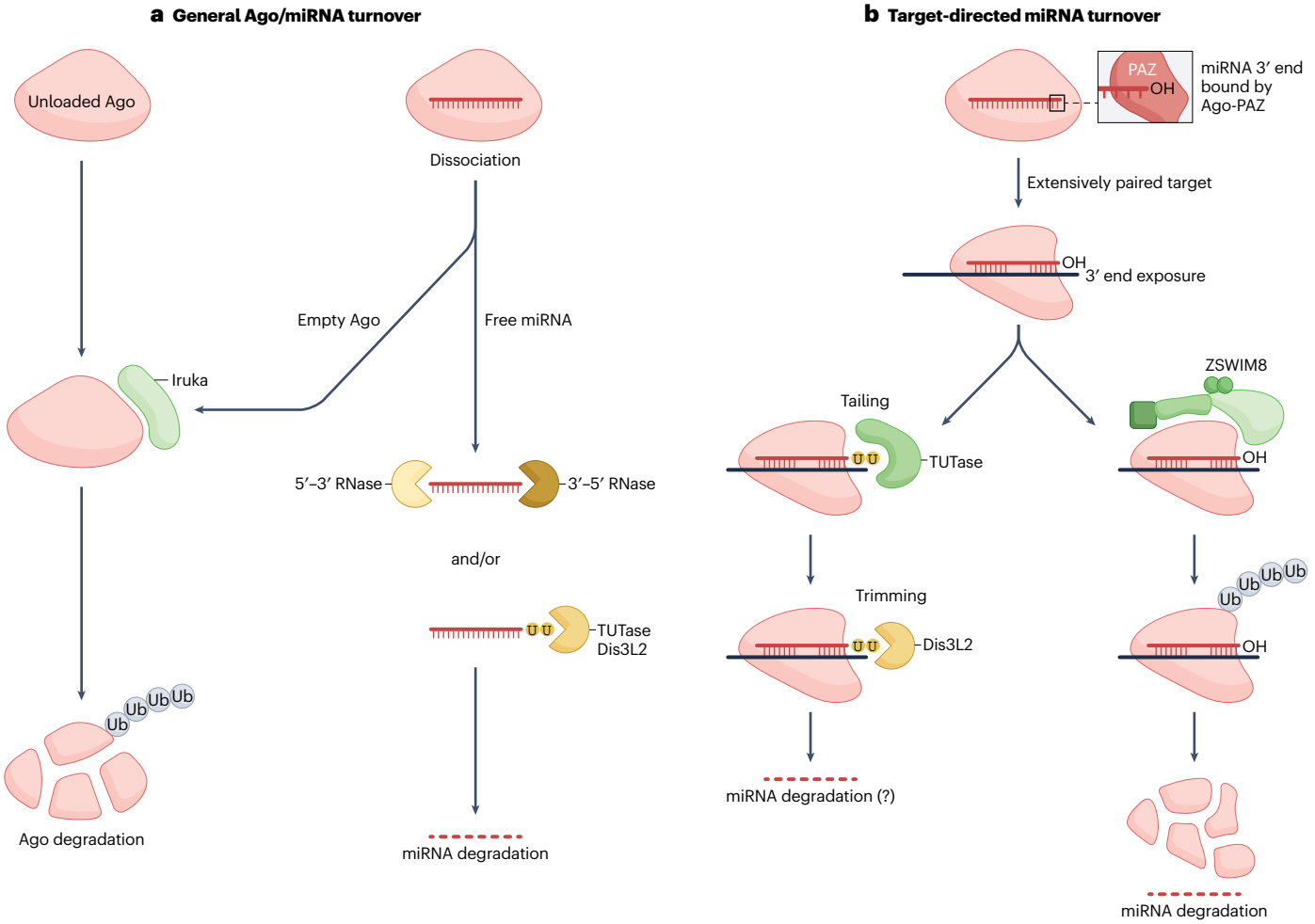

Fig. 5 | Regulation of miRNA turnover. a, General turnover of Argonaute (Ago)–microRNA (miRNA) complexes. Ago proteins that are not associated with small RNAs are usually unstable and selectively degraded across species. In principle, these exist prior to miRNA loading or after ejection of the mature miRNA. Empty Ago proteins are selectively tagged by the E3 ubiquitin ligase Iruka, which signals its degradation by the proteasome. In concert, miRNAs are generally stable within Ago complexes. However, when not shielded by Ago protein, miRNAs are generally unstable as they lack 5′ cap and 3′ polyA tails. Such free miRNAs may be degraded directly by various exoribonucleolytic pathways or may be subject to 3′ tailing by terminal uridyltransferases (TUTases) and degradation by Dis3L2 3′ exoribonuclease. **b**, Target-directed miRNA degradation (TDMD) is a sequence-specific process by which individual designated miRNAs are degraded upon interaction with highly complementary trigger RNAs. Normally, the miRNA 3′ end is bound by the Ago-PAZ domain. However, when engaged in extensive base-pairing with a TDMD trigger, the miRNA 3′ end is exposed. This provides access to modification by TUTase and potential degradation by Dis3L2; however, tailing is not generally coupled to turnover. Instead, the dominant mechanism for TDMD involves a conformational change of Ago that allows it to be selectively recognized by ZSWIM8, which recruits a Cullin–RING E3 ubiquitin ligase complex to degrade Ago. The exposed miRNA is then presumably subject to turnover by general exoribonucleases.

structure, mediated by a conserved loop motif and the dsRBD factor ILF3 (ref. 211). Undoubtedly, additional mechanisms of positive and negative regulation in miRNA biogenesis will be elucidated in the future.

Finally, we must not lose sight of the implications of miRNA biology, such as whether the regulation of defined miRNA targets truly mediate organismal phenotypes. To date, most studies of miRNA–target biology remain correlative, and the mere fact that numerous derepressed targets can be detected upon miRNA loss does not necessarily mean they all contribute functionally to miRNA phenotypes. Recently, CRISPR mutagenesis has validated a growing number of TDMD target sites that genuinely restrict miRNA abundance[197,200,201] (Fig. 5), as well as demonstrated the strong phenotypic impact of target mRNAs via defined miRNA sites[212–215]. Ultimately, achieving such direct connections between target site-mediated gene regulation and in vivo phenotypes are required to fully understand miRNA function in development and disease.

Published online: 28 June 2023

References

1. Lee, R. C., Feinbaum, R. L. & Ambros, V. The *C. elegans* heterochronic gene *lin-4* encodes small RNAs with antisense complementarity to *lin-14*. *Cell* **75**, 843–854 (1993).
2. Wightman, B., Ha, I. & Ruvkun, G. Posttranscriptional regulation of the heterochronic gene *lin-14* by *lin-4* mediates temporal pattern formation in *C. elegans*. *Cell* **75**, 855–862 (1993).

3. Leviten, M. W., Lai, E. C. & Posakony, J. W. The *Drosophila* gene *Bearded* encodes a novel small protein and shares 3′ UTR sequence motifs with multiple *Enhancer of split* complex genes. *Development* **124**, 4039–4051 (1997).
4. Lai, E. C. & Posakony, J. W. The Bearded box, a novel 3′ UTR sequence motif, mediates negative post-transcriptional regulation of *Bearded* and *Enhancer of split* complex gene expression. *Development* **124**, 4847–4856 (1997).
5. Lai, E. C., Burks, C. & Posakony, J. W. The K box, a conserved 3′ UTR sequence motif, negatively regulates accumulation of *Enhancer of split* complex transcripts. *Development* **125**, 4077–4088 (1998).
6. Lai, E. C. microRNAs are complementary to 3′ UTR sequence motifs that mediate negative post-transcriptional regulation. *Nat. Genet.* **30**, 363–364 (2002).
7. Lau, N., Lim, L., Weinstein, E. & Bartel, D. P. An abundant class of tiny RNAs with probable regulatory roles in *Caenorhabditis elegans*. *Science* **294**, 858–862 (2001).
8. Lee, R. C. & Ambros, V. An extensive class of small RNAs in *Caenorhabditis elegans*. *Science* **294**, 862–864 (2001).
9. Lagos-Quintana, M., Rauhut, R., Lendeckel, W. & Tuschl, T. Identification of novel genes coding for small expressed RNAs. *Science* **294**, 853–858 (2001).
10. Bartel, D. P. Metazoan microRNAs. *Cell* **173**, 20–51 (2018).
11. Czech, B. & Hannon, G. J. Small RNA sorting: matchmaking for Argonautes. *Nat. Rev. Genet.* **12**, 19–31 (2010).
12. Yang, J. S. & Lai, E. C. Alternative miRNA biogenesis pathways and the interpretation of core miRNA pathway mutants. *Mol. Cell* **43**, 892–903 (2011).
13. Maurin, T., Cazalla, D., Yang, J. S., Bortolamiol-Becet, D. & Lai, E. C. RNase III-independent microRNA biogenesis in mammalian cells. *RNA* **18**, 2166–2173 (2012).
14. Shang, R. et al. Ribozyme-enhanced single-stranded Ago2-processed interfering RNA triggers efficient gene silencing with fewer off-target effects. *Nat. Commun.* **6**, 8430 (2015).
15. Lai, E. C., Tam, B. & Rubin, G. M. Pervasive regulation of *Drosophila* Notch target genes by GY-box-, Brd-box-, and K-box-class microRNAs. *Genes Dev.* **19**, 1067–1080 (2005).
16. Lewis, B. P., Burge, C. B. & Bartel, D. P. Conserved seed pairing, often flanked by adenosines, indicates that thousands of human genes are microRNA targets. *Cell* **120**, 15–20 (2005).
17. Brennecke, J., Stark, A., Russell, R. B. & Cohen, S. M. Principles of microRNA–target recognition. *PLoS Biol.* **3**, e85 (2005).
18. Wang, Y., Sheng, G., Juranek, S., Tuschl, T. & Patel, D. J. Structure of the guide-strand-containing Argonaute silencing complex. *Nature* **456**, 209–213 (2008).
19. Schirle, N. T. & MacRae, I. J. The crystal structure of human Argonaute2. *Science* **336**, 1037–1040 (2012).
20. Elkayam, E. et al. The structure of human Argonaute-2 in complex with miR-20a. *Cell* **150**, 100–110 (2012).
21. Liu, J. et al. Argonaute2 is the catalytic engine of mammalian RNAi. *Science* **305**, 1437–1441 (2004).
22. Meister, G. et al. Human Argonaute2 mediates RNA cleavage targeted by miRNAs and siRNAs. *Mol. Cell* **15**, 185–197 (2004).
23. Park, M. S. et al. Human Argonaute3 has slicer activity. *Nucleic acids Res.* **45**, 11867–11877 (2017).
24. Park, M. S., Sim, G., Kehling, A. C. & Nakanishi, K. Human Argonaute2 and Argonaute3 are catalytically activated by different lengths of guide RNA. *Proc. Natl Acad. Sci. USA* **117**, 28576–28578 (2020).
25. Nguyen, H. M., Nguyen, T. D., Nguyen, T. L. & Nguyen, T. A. Orientation of human microprocessor on primary microRNAs. *Biochemistry* **58**, 189–198 (2019).
26. Han, J. et al. Molecular basis for the recognition of primary microRNAs by the Drosha–DGCR8 complex. *Cell* **125**, 887–901 (2006).
27. Zeng, Y. & Cullen, B. R. Efficient processing of primary microRNA hairpins by Drosha requires flanking non-structured RNA sequences. *J. Biol. Chem.* **280**, 27595–27603 (2005).
28. Zeng, Y., Yi, R. & Cullen, B. R. Recognition and cleavage of primary microRNA precursors by the nuclear processing enzyme Drosha. *EMBO J.* **24**, 138–148 (2005).
29. Ma, H., Wu, Y., Choi, J. G. & Wu, H. Lower and upper stem-single-stranded RNA junctions together determine the Drosha cleavage site. *Proc. Natl Acad. Sci. USA* **110**, 20687–20692 (2013).
30. Auyeung, V. C., Ulitsky, I., McGeary, S. E. & Bartel, D. P. Beyond secondary structure: primary-sequence determinants license pri-miRNA hairpins for processing. *Cell* **152**, 844–858 (2013).
This study is the first to utilize massively parallel substrate assays to reveal motifs involved in pri-miRNA processing.
31. Fang, W. & Bartel, D. P. The menu of features that define primary microRNAs and enable de novo design of microRNA genes. *Mol. Cell* **60**, 131–145 (2015).
32. Partin, A. C. et al. Heme enables proper positioning of Drosha and DGCR8 on primary microRNAs. *Nat. Commun.* **8**, 1737 (2017).
33. Nguyen, T. A., Park, J., Dang, T. L., Choi, Y. G. & Kim, V. N. Microprocessor depends on hemin to recognize the apical loop of primary microRNA. *Nucleic acids Res.* **46**, 5726–5736 (2018).
34. Kim, K., Nguyen, T. D., Li, S. & Nguyen, T. A. SRSF3 recruits DROSHA to the basal junction of primary microRNAs. *RNA* **24**, 892–898 (2018).
35. Fernandez, N. et al. Genetic variation and RNA structure regulate microRNA biogenesis. *Nat. Commun.* **8**, 15114 (2017).
36. Li, S., Nguyen, T. D., Nguyen, T. L. & Nguyen, T. A. Mismatched and wobble base pairs govern primary microRNA processing by human microprocessor. *Nat. Commun.* **11**, 1926 (2020).
37. Li, S., Le, T. N., Nguyen, T. D., Trinh, T. A. & Nguyen, T. A. Bulges control pri-miRNA processing in a position and strand-dependent manner. *RNA Biol.* **18**, 1716–1726 (2021).
38. Lee, Y. Y., Kim, H. & Kim, V. N. Sequence determinant of small RNA production by DICER. *Nature* **615**, 323–330 (2023).
39. Rice, G. M., Shivashankar, V., Ma, E. J., Baryza, J. L. & Nutiu, R. Functional atlas of primary miRNA maturation by the microprocessor. *Mol. Cell* **80**, 892–902.e4 (2020).
40. Kim, K. et al. A quantitative map of human primary microRNA processing sites. *Mol. Cell* **81**, 3422–3439.e11 (2021).
41. Kang, W. et al. MapToCleave: high-throughput profiling of microRNA biogenesis in living cells. *Cell Rep.* **37**, 110015 (2021).
42. Chiang, H. R. et al. Mammalian microRNAs: experimental evaluation of novel and previously annotated genes. *Genes Dev.* **24**, 992–1009 (2010).
43. Consortium, R. RNAcentral 2021: secondary structure integration, improved sequence search and new member databases. *Nucleic acids Res.* **49**, D212–D220 (2021).
44. Fromm, B., Zhong, X., Tarbier, M., Friedlander, M. R. & Hackenberg, M. The limits of human microRNA annotation have been met. *RNA* https://doi.org/10.1261/rna.079098.122 (2022).
45. Nguyen, T. L., Nguyen, T. D., Bao, S., Li, S. & Nguyen, T. A. The internal loops in the lower stem of primary microRNA transcripts facilitate single cleavage of human microprocessor. *Nucleic acids Res.* **48**, 2579–2593 (2020).
46. Luo, Q. J. et al. RNA structure probing reveals the structural basis of Dicer binding and cleavage. *Nat. Commun.* **12**, 3397 (2021).
47. Zhang, H., Kolb, F. A., Jaskiewicz, L., Westhof, E. & Filipowicz, W. Single processing center models for human Dicer and bacterial RNase III. *Cell* **118**, 57–68 (2004).
48. Macrae, I. J. et al. Structural basis for double-stranded RNA processing by Dicer. *Science* **311**, 195–198 (2006).
49. MacRae, I. J., Zhou, K. & Doudna, J. A. Structural determinants of RNA recognition and cleavage by Dicer. *Nat. Struct. Mol. Biol.* **14**, 934–940 (2007).
50. Vermeulen, A. et al. The contributions of dsRNA structure to Dicer specificity and efficiency. *RNA* **11**, 674–682 (2005).
51. Zhang, H., Kolb, F. A., Brondani, V., Billy, E. & Filipowicz, W. Human Dicer preferentially cleaves dsRNAs at their termini without a requirement for ATP. *EMBO J.* **21**, 5875–5885 (2002).
52. Park, J. E. et al. Dicer recognizes the 5′ end of RNA for efficient and accurate processing. *Nature* **475**, 201–205 (2011).
53. Gu, S. et al. The loop position of shRNAs and pre-miRNAs is critical for the accuracy of dicer processing in vivo. *Cell* **151**, 900–911 (2012).
54. Nguyen, T. D., Trinh, T. A., Bao, S. & Nguyen, T. A. Secondary structure RNA elements control the cleavage activity of DICER. *Nat. Commun.* **13**, 2138 (2022).
55. Frank, F., Sonenberg, N. & Nagar, B. Structural basis for 5′-nucleotide base-specific recognition of guide RNA by human AGO2. *Nature* **465**, 818–822 (2010).
56. Boland, A., Tritschler, F., Heimstadt, S., Izaurralde, E. & Weichenrieder, O. Crystal structure and ligand binding of the MID domain of a eukaryotic Argonaute protein. *EMBO Rep.* **11**, 522–527 (2010).
57. Schirle, N. T., Sheu-Gruttadauria, J., Chandradoss, S. D., Joo, C. & MacRae, I. J. Water-mediated recognition of t1-adenosine anchors Argonaute2 to microRNA targets. *eLife* https://doi.org/10.7554/eLife.07646 (2015).
58. Shin, C. et al. Expanding the microRNA targeting code: functional sites with centered pairing. *Mol. Cell* **38**, 789–802 (2010).
59. Chi, S. W., Hannon, G. J. & Darnell, R. B. An alternative mode of microRNA target recognition. *Nat. Struct. Mol. Biol.* **19**, 321–327 (2012).
60. Lal, A. et al. miR-24 Inhibits cell proliferation by targeting E2F2, MYC, and other cell-cycle genes via binding to "seedless" 3′UTR microRNA recognition elements. *Mol. Cell* **35**, 610–625 (2009).
61. Loeb, G. B. et al. Transcriptome-wide miR-155 binding map reveals widespread noncanonical microRNA targeting. *Mol. Cell* **48**, 760–770 (2012).
62. Hafner, M. et al. Transcriptome-wide identification of RNA-binding protein and microRNA target sites by PAR-CLIP. *Cell* **141**, 129–141 (2010).
63. Becker, W. R. et al. High-throughput analysis reveals rules for target RNA binding and cleavage by AGO2. *Mol. Cell* **75**, 741–755.e11 (2019).
64. McGeary, S. E. et al. The biochemical basis of microRNA targeting efficacy. *Science* https://doi.org/10.1126/science.aav1741 (2019).
This paper reveals broad features of miRNA–target interactions using RBNS.
65. McGeary, S. E., Bisaria, N., Pham, T. M., Wang, P. Y. & Bartel, D. P. microRNA 3′-compensatory pairing occurs through two binding modes, with affinity shaped by nucleotide identity and position. *eLife* https://doi.org/10.7554/eLife.69803 (2022).
66. Grimson, A. et al. microRNA targeting specificity in mammals: determinants beyond seed pairing. *Mol. Cell* **27**, 91–105 (2007).
67. Gu, S., Jin, L., Zhang, F., Sarnow, P. & Kay, M. A. Biological basis for restriction of microRNA targets to the 3′ untranslated region in mammalian mRNAs. *Nat. Struct. Mol. Biol.* **16**, 144–150 (2009).
68. Schnall-Levin, M. et al. Unusually effective microRNA targeting within repeat-rich coding regions of mammalian mRNAs. *Genome Res.* **21**, 1395–1403 (2011).
69. Zhang, K. et al. A novel class of microRNA-recognition elements that function only within open reading frames. *Nat. Struct. Mol. Biol.* **25**, 1019–1027 (2018).
70. Yu, S. & Kim, V. N. A tale of non-canonical tails: gene regulation by post-transcriptional RNA tailing. *Nat. Rev. Mol. Cell Biol.* https://doi.org/10.1038/s41580-020-0246-8 (2020).
71. Yang, A. et al. 3′ uridylation confers miRNAs with non-canonical target repertoires. *Mol. Cell* **75**, 511–522.e4 (2019).

72. Sheu-Gruttadauria, J., Xiao, Y., Gebert, L. F. & MacRae, I. J. Beyond the seed: structural basis for supplementary microRNA targeting by human Argonaute2. *EMBO J.* **38**, e101153 (2019).
73. Sim, G. et al. Manganese-dependent microRNA trimming by 3′→5′ exonucleases generates 14-nucleotide or shorter tiny RNAs. *Proc. Natl Acad. Sci. USA* **119**, e2214335119 (2022).
74. Kim, H. H. et al. HuR recruits let-7/RISC to repress c-Myc expression. *Genes Dev.* **23**, 1743–1748 (2009).
75. Sternburg, E. L., Estep, J. A., Nguyen, D. K., Li, Y. & Karginov, F. V. Antagonistic and cooperative AGO2–PUM interactions in regulating mRNAs. *Sci. Rep.* **8**, 15316 (2018).
76. Kedde, M. et al. RNA-binding protein Dnd1 inhibits microRNA access to target mRNA. *Cell* **131**, 1273–1286 (2007).
77. Kim, S. et al. The regulatory impact of RNA-binding proteins on microRNA targeting. *Nat. Commun.* **12**, 5057 (2021).
78. Wang, Y. et al. Structure of an argonaute silencing complex with a seed-containing guide DNA and target RNA duplex. *Nature* **456**, 921–926 (2008).
79. Wang, Y. et al. Nucleation, propagation and cleavage of target RNAs in Ago silencing complexes. *Nature* **461**, 754–761 (2009).
80. Song, J. J., Smith, S. K., Hannon, G. J. & Joshua-Tor, L. Crystal structure of Argonaute and its implications for RISC slicer activity. *Science* **305**, 1434–1437 (2004).
81. Liu, Z. et al. Cryo-EM structure of human dicer and its complexes with a pre-miRNA substrate. *Cell* **173**, 1191–1203.e12 (2018).
82. Nguyen, T. A. et al. Functional anatomy of the human microprocessor. *Cell* **161**, 1374–1387 (2015).
83. Kwon, S. C. et al. Structure of human DROSHA. *Cell* **164**, 81–90 (2016).
84. Barr, I. et al. DiGeorge critical region 8 (DGCR8) is a double-cysteine-ligated heme protein. *J. Biol. Chem.* **286**, 16716–16725 (2011).
85. Quick-Cleveland, J. et al. The DGCR8 RNA-binding heme domain recognizes primary microRNAs by clamping the hairpin. *Cell Rep.* **7**, 1994–2005 (2014).
86. Jin, W., Wang, J., Liu, C. P., Wang, H. W. & Xu, R. M. Structural basis for pri-miRNA recognition by Drosha. *Mol. Cell* **78**, 423–433.e5 (2020).
87. Partin, A. C. et al. Cryo-EM structures of human Drosha and DGCR8 in complex with primary microRNA. *Mol. Cell* **78**, 411–422 e414 (2020).
Together with Jin et al. (2020), this work is the first cryo-EM study of Microprocessor structures.
88. Shi, Z., Nicholson, R. H., Jaggi, R. & Nicholson, A. W. Characterization of Aquifex aeolicus ribonuclease III and the reactivity epitopes of its pre-ribosomal RNA substrates. *Nucleic acids Res.* **39**, 2756–2768 (2011).
89. Carmell, M. A. & Hannon, G. J. RNase III enzymes and the initiation of gene silencing. *Nat. Struct. Mol. Biol.* **11**, 214–218 (2004).
90. Lee, Y. Y., Lee, H., Kim, H., Kim, V. N. & Roh, S. H. Structure of the human DICER–pre-miRNA complex in a dicing state. *Nature* **615**, 331–338 (2023).
91. Zapletal, D. et al. Structural and functional basis of mammalian microRNA biogenesis by Dicer. *Mol. Cell* **82**, 4064–4079.e13 (2022).
Together with Lee et al. (*Nature*, 2023), this work reports new cryo-EM structures for active mammalian Dicer complex.
92. Jouravleva, K. et al. Structural basis of microRNA biogenesis by Dicer-1 and its partner protein Loqs-PB. *Mol. Cell* **82**, 4049–4063.e6 (2022).
93. Wei, X. et al. Structural basis of microRNA processing by Dicer-like 1. *Nat. Plants* **7**, 1389–1396 (2021).
94. Fareh, M. et al. TRBP ensures efficient Dicer processing of precursor microRNA in RNA-crowded environments. *Nat. Commun.* **7**, 13694 (2016).
95. Yamaguchi, S. et al. Structure of the Dicer-2–R2D2 heterodimer bound to a small RNA duplex. *Nature* **607**, 393–398 (2022).
96. Su, S. et al. Structural insights into dsRNA processing by *Drosophila* Dicer-2–Loqs-PD. *Nature* **607**, 399–406 (2022).
97. Wang, Q. et al. Mechanism of siRNA production by a plant Dicer–RNA complex in dicing-competent conformation. *Science* **374**, 1152–1157 (2021).
98. Herbert, K. M. et al. A heterotrimer model of the complete Microprocessor complex revealed by single-molecule subunit counting. *RNA* **22**, 175–183 (2016).
99. Naganuma, M., Tadakuma, H. & Tomari, Y. Single-molecule analysis of processive double-stranded RNA cleavage by *Drosophila* Dicer-2. *Nat. Commun.* **12**, 4268 (2021).
100. Iwasaki, S. et al. Defining fundamental steps in the assembly of the *Drosophila* RNAi enzyme complex. *Nature* **521**, 533–536 (2015).
101. Tsuboyama, K., Tadakuma, H. & Tomari, Y. Conformational activation of argonaute by distinct yet coordinated actions of the Hsp70 and Hsp90 chaperone systems. *Mol. Cell* **70**, 722–729.e4 (2018).
102. Willkomm, S. et al. Single-molecule FRET uncovers hidden conformations and dynamics of human Argonaute 2. *Nat. Commun.* **13**, 3825 (2022).
This study uses single-molecule fluorescence to dissect internal motions within human Ago2 during transitions from guide RNA binding to target capture.
103. Salomon, W. E., Jolly, S. M., Moore, M. J., Zamore, P. D. & Serebrov, V. Single-molecule imaging reveals that argonaute reshapes the binding properties of its nucleic acid guides. *Cell* **162**, 84–95 (2015).
104. Yao, C., Sasaki, H. M., Ueda, T., Tomari, Y. & Tadakuma, H. Single-molecule analysis of the target cleavage reaction by the *Drosophila* RNAi enzyme complex. *Mol. Cell* **59**, 125–132 (2015).
105. Chandradoss, S. D., Schirle, N. T., Szczepaniak, M., MacRae, I. J. & Joo, C. A dynamic search process underlies microRNA targeting. *Cell* **162**, 96–107 (2015).
This study uses the distance sensing capability of smFRET to visualize strategies of target interrogation by RISC.
106. Klum, S. M., Chandradoss, S. D., Schirle, N. T., Joo, C. & MacRae, I. J. Helix-7 in argonaute2 shapes the microRNA seed region for rapid target recognition. *EMBO J.* **37**, 75–88 (2018).
107. Cui, T. J. et al. Argonaute bypasses cellular obstacles without hindrance during target search. *Nat. Commun.* **10**, 4390 (2019).
108. Ruijtenberg, S. et al. mRNA structural dynamics shape Argonaute–target interactions. *Nat. Struct. Mol. Biol.* **27**, 790–801 (2020).
109. Cialek, C. A. et al. Imaging translational control by Argonaute with single-molecule resolution in live cells. *Nat. Commun.* **13**, 3345 (2022).
110. Kobayashi, H. & Singer, R. H. Single-molecule imaging of microRNA-mediated gene silencing in cells. *Nat. Commun.* **13**, 1435 (2022).
111. Sheu-Gruttadauria, J. & MacRae, I. J. Structural foundations of RNA silencing by Argonaute. *J. Mol. Biol.* **429**, 2619–2639 (2017).
112. Nakanishi, K. Anatomy of four human Argonaute proteins. *Nucleic acids Res.* **50**, 6618–6638 (2022).
113. Sheu-Gruttadauria, J. et al. Structural basis for target-directed microRNA degradation. *Mol. Cell* https://doi.org/10.1016/j.molcel.2019.06.019 (2019).
114. Newman, M. A., Thomson, J. M. & Hammond, S. M. Lin-28 interaction with the Let-7 precursor loop mediates regulated microRNA processing. *RNA* **14**, 1539–1549 (2008).
115. Heo, I. et al. Lin28 mediates the terminal uridylation of let-7 precursor microRNA. *Mol. Cell* **32**, 276–284 (2008).
116. Viswanathan, S. R., Daley, G. Q. & Gregory, R. I. Selective blockade of microRNA processing by Lin28. *Science* **320**, 97–100 (2008).
117. Rybak, A. et al. A feedback loop comprising lin-28 and let-7 controls pre-let-7 maturation during neural stem-cell commitment. *Nat. Cell Biol.* **10**, 987–993 (2008).
118. Heo, I. et al. TUT4 in concert with Lin28 suppresses microRNA biogenesis through pre-microRNA uridylation. *Cell* **138**, 696–708 (2009).
119. Thornton, J. E., Chang, H. M., Piskounova, E. & Gregory, R. I. Lin28-mediated control of let-7 microRNA expression by alternative TUTases Zcchc11 (TUT4) and Zcchc6 (TUT7). *RNA* **18**, 1875–1885 (2012).
120. Chang, H. M., Triboulet, R., Thornton, J. E. & Gregory, R. I. A role for the Perlman syndrome exonuclease Dis3l2 in the Lin28–let-7 pathway. *Nature* https://doi.org/10.1038/nature12119 (2013).
121. Faehnle, C. R., Walleshauser, J. & Joshua-Tor, L. Mechanism of Dis3l2 substrate recognition in the Lin28–let-7 pathway. *Nature* **514**, 252–256 (2014).
122. Ustianenko, D. et al. Mammalian DIS3L2 exoribonuclease targets the uridylated precursors of let-7 miRNAs. *RNA* **19**, 1632–1638 (2013).
123. Heo, I. et al. Mono-uridylation of pre-microRNA as a key step in the biogenesis of group II let-7 microRNAs. *Cell* **151**, 521–532 (2012).
124. Kim, H. et al. A mechanism for microRNA arm switching regulated by uridylation. *Mol. Cell* **78**, 1224–1236.e5 (2020).
125. Michlewski, G. & Caceres, J. F. Post-transcriptional control of miRNA biogenesis. *RNA* **25**, 1–16 (2019).
126. Treiber, T., Treiber, N. & Meister, G. Regulation of microRNA biogenesis and its crosstalk with other cellular pathways. *Nat. Rev. Mol. Cell Biol.* **20**, 5–20 (2019).
127. Michlewski, G., Guil, S., Semple, C. A. & Caceres, J. F. Posttranscriptional regulation of miRNAs harboring conserved terminal loops. *Mol. Cell* **32**, 383–393 (2008).
128. Nussbacher, J. K. & Yeo, G. W. Systematic discovery of RNA binding proteins that regulate microRNA levels. *Mol. Cell* **69**, 1005–1016.e7 (2018).
129. Treiber, T. et al. A compendium of RNA-binding proteins that regulate microRNA biogenesis. *Mol. Cell* **66**, 270–284.e13 (2017).
130. Tokumaru, S., Suzuki, M., Yamada, H., Nagino, M. & Takahashi, T. let-7 regulates Dicer expression and constitutes a negative feedback loop. *Carcinogenesis* **29**, 2073–2077 (2008).
131. Martello, G. et al. A microRNA targeting dicer for metastasis control. *Cell* **141**, 1195–1207 (2010).
132. Wang, D. et al. Uncovering the cellular capacity for intensive and specific feedback self-control of the argonautes and microRNA targeting activity. *Nucleic acids Res.* **48**, 4681–4697 (2020).
133. Smibert, P., Yang, J. S., Azzam, G., Liu, J. L. & Lai, E. C. Homeostatic control of Argonaute stability by microRNA availability. *Nat. Struct. Mol. Biol.* **20**, 789–795 (2013).
134. Kobayashi, H., Shoji, K., Kiyokawa, K., Negishi, L. & Tomari, Y. Iruka eliminates dysfunctional argonaute by selective ubiquitination of its empty state. *Mol. Cell* **73**, 119–129.e5 (2019).
135. Martinez, N. J. & Gregory, R. I. Argonaute2 expression is post-transcriptionally coupled to microRNA abundance. *RNA* **19**, 605–612 (2013).
136. Derrien, B. et al. Degradation of the antiviral component ARGONAUTE1 by the autophagy pathway. *Proc. Natl Acad. Sci. USA* **109**, 15942–15946 (2012).
137. Han, J. et al. Posttranscriptional crossregulation between Drosha and DGCR8. *Cell* **136**, 75–84 (2009).
This paper identifies the first cross-regulations between miRNA factors, in this case between Microprocessor components Drosha and DGCR8 (see also references 138 and 139).
138. Kadener, S. et al. Genome-wide identification of targets of the Drosha-Pasha/DGCR8 complex. *RNA* **15**, 537–545 (2009).
139. Smibert, P. et al. A *Drosophila* genetic screen yields allelic series of core microRNA biogenesis factors and reveals post-developmental roles for microRNAs. *RNA* **17**, 1997–2010 (2011).
140. Cui, Y. et al. Global miRNA dosage control of embryonic germ layer specification. *Nature* **593**, 602–606 (2021).

141. Baskerville, S. & Bartel, D. P. Microarray profiling of microRNAs reveals frequent coexpression with neighboring miRNAs and host genes. *RNA* **11**, 241–247 (2005).
142. Du, P., Wang, L., Sliz, P. & Gregory, R. I. A biogenesis step upstream of microprocessor controls miR-17 approximately 92 expression. *Cell* **162**, 885–899 (2015).
143. Donayo, A. O. et al. Oncogenic biogenesis of pri-miR-17-92 reveals hierarchy and competition among polycistronic microRNAs. *Mol. Cell* **75**, 340–356 (2019).
144. Truscott, M., Islam, A. B. & Frolov, M. V. Novel regulation and functional interaction of polycistronic miRNAs. *RNA* **22**, 129–138 (2016).
145. Lataniotis, L. et al. CRISPR/Cas9 editing reveals novel mechanisms of clustered microRNA regulation and function. *Sci. Rep.* **7**, 8585 (2017).
146. Haar, J. et al. The expression of a viral microRNA is regulated by clustering to allow optimal B cell transformation. *Nucleic acids Res.* **44**, 1326–1341 (2016).
147. Vilimova, M. et al. *Cis* regulation within a cluster of viral microRNAs. *Nucleic acids Res.* **49**, 10018–10033 (2021).
148. Yang, J. S. & Lai, E. C. Dicer-independent, Ago2-mediated microRNA biogenesis in vertebrates. *Cell Cycle* **9**, 4455–4460 (2010).
149. Jee, D. et al. Dual strategies for Argonaute2-mediated biogenesis of erythroid miRNAs underlie conserved requirements for slicing in mammals. *Mol. Cell* **69**, 265–278.e6 (2018).
150. Kretov, D. A. et al. Ago2-dependent processing allows miR-451 to evade the global microRNA turnover elicited during erythropoiesis. *Mol. Cell* **78**, 317–328.e6 (2020).
151. Shang, R. et al. Genomic clustering facilitates nuclear processing of suboptimal pri-miRNA loci. *Mol. Cell* **78**, 303–316.e4 (2020).
152. Fang, W. & Bartel, D. P. microRNA clustering assists processing of suboptimal microRNA hairpins through the action of the ERH protein. *Mol. Cell* **78**, 289–302.e6 (2020).
153. Hutter, K. et al. SAFB2 enables the processing of suboptimal stem–loop structures in clustered primary miRNA transcripts. *Mol. Cell* **78**, 876–889 (2020).
Together with Shang et al. (2020) and Fang and Bartel (2020), this work reports mechanisms for miRNA cluster assistance for suboptimal miRNA biogenesis.
154. Kwon, S. C. et al. ERH facilitates microRNA maturation through the interaction with the N-terminus of DGCR8. *Nucleic acids Res.* **48**, 11097–11112 (2020).
155. Kim, Y. K. & Kim, V. N. Processing of intronic microRNAs. *EMBO J.* **26**, 775–783 (2007).
156. Ballarino, M. et al. Coupled RNA processing and transcription of intergenic primary microRNAs. *Mol. Cell. Biol.* **29**, 5632–5638 (2009).
157. Morlando, M. et al. Primary microRNA transcripts are processed co-transcriptionally. *Nat. Struct. Mol. Biol.* **15**, 902–909 (2008).
158. Liu, H. et al. HP1BP3, a chromatin retention factor for co-transcriptional microRNA processing. *Mol. Cell* **63**, 420–432 (2016).
159. Church, V. A. et al. Microprocessor recruitment to elongating RNA polymerase II is required for differential expression of microRNAs. *Cell Rep.* **20**, 3123–3134 (2017).
160. Pawlicki, J. M. & Steitz, J. A. Primary microRNA transcript retention at sites of transcription leads to enhanced microRNA production. *J. Cell Biol.* **182**, 61–76 (2008).
161. Bernstein, E., Caudy, A., Hammond, S. & Hannon, G. Role for a bidentate ribonuclease in the initiation step of RNA interference. *Nature* **409**, 363–366 (2001).
162. Hutvagner, G. et al. A cellular function for the RNA-interference enzyme Dicer in the maturation of the *let-7* small temporal RNA. *Science* **293**, 834–838 (2001).
163. Flemr, M. et al. A retrotransposon-driven dicer isoform directs endogenous small interfering RNA production in mouse oocytes. *Cell* **155**, 807–816 (2013).
This paper reports that an endogenous N-terminally truncated Dicer isoform processes siRNAs in mouse oocytes, an unusual setting for mammalian siRNA biology.
164. Watanabe, T. et al. Endogenous siRNAs from naturally formed dsRNAs regulate transcripts in mouse oocytes. *Nature* **453**, 539–543 (2008).
165. Tam, O. H. et al. Pseudogene-derived small interfering RNAs regulate gene expression in mouse oocytes. *Nature* **453**, 534–538 (2008).
166. Suh, N. et al. microRNA function is globally suppressed in mouse oocytes and early embryos. *Curr. Biol.* **20**, 271–277 (2010).
167. Murchison, E. P. et al. Critical roles for Dicer in the female germline. *Genes Dev.* **21**, 682–693 (2007).
168. Kataruka, S. et al. microRNA dilution during oocyte growth disables the microRNA pathway in mammalian oocytes. *Nucleic acids Res.* **48**, 8050–8062 (2020).
169. Schuster, S., Miesen, P. & van Rij, R. P. Antiviral RNAi in insects and mammals: parallels and differences. *Viruses* https://doi.org/10.3390/v11050448 (2019).
170. Kennedy, E. M. et al. Production of functional small interfering RNAs by an amino-terminal deletion mutant of human Dicer. *Proc. Natl Acad. Sci. USA* **112**, E6945–E6954 (2015).
171. Poirier, E. Z. et al. An isoform of Dicer protects mammalian stem cells against multiple RNA viruses. *Science* **373**, 231–236 (2021).
172. Li, Y., Lu, J., Han, Y., Fan, X. & Ding, S. W. RNA interference functions as an antiviral immunity mechanism in mammals. *Science* **342**, 231–234 (2013).
173. Maillard, P. V. et al. Antiviral RNA interference in mammalian cells. *Science* **342**, 235–238 (2013).
174. Gantier, M. P. et al. Analysis of microRNA turnover in mammalian cells following Dicer1 ablation. *Nucleic acids Res.* **39**, 5692–5703 (2011).
175. van Rooij, E. et al. Control of stress-dependent cardiac growth and gene expression by a microRNA. *Science* **316**, 575–579 (2007).
176. Kingston, E. R. & Bartel, D. P. Global analyses of the dynamics of mammalian microRNA metabolism. *Genome Res.* **29**, 1777–1790 (2019).
177. Gibbings, D. et al. Selective autophagy degrades DICER and AGO2 and regulates miRNA activity. *Nat. Cell Biol.* **14**, 1314–1321 (2012).
178. Reichholf, B. et al. Time-resolved small RNA sequencing unravels the molecular principles of microRNA homeostasis. *Mol. Cell* **75**, 756–768.e7 (2019).
179. Krol, J. et al. Characterizing light-regulated retinal microRNAs reveals rapid turnover as a common property of neuronal microRNAs. *Cell* **141**, 618–631 (2010).
180. Ramachandran, V. & Chen, X. Degradation of microRNAs by a family of exoribonucleases in *Arabidopsis*. *Science* **321**, 1490–1492 (2008).
181. Shukla, S., Bjerke, G. A., Muhlrad, D., Yi, R. & Parker, R. The RNase PARN controls the levels of specific miRNAs that contribute to p53 regulation. *Mol. Cell* **73**, 1204–1216.e4 (2019).
182. Yu, Y. et al. ARGONAUTE10 promotes the degradation of miR165/6 through the SDN1 and SDN2 exonucleases in *Arabidopsis*. *PLoS Biol.* **15**, e2001272 (2017).
183. Ibrahim, F. et al. Uridylation of mature miRNAs and siRNAs by the MUT68 nucleotidyltransferase promotes their degradation in *Chlamydomonas*. *Proc. Natl Acad. Sci. USA* **107**, 3906–3911 (2010).
184. Chatterjee, S. & Grosshans, H. Active turnover modulates mature microRNA activity in *Caenorhabditis elegans*. *Nature* **461**, 546–549 (2009).
185. Cazalla, D., Yario, T. & Steitz, J. A. Down-regulation of a host microRNA by a *Herpesvirus saimiri* noncoding RNA. *Science* **328**, 1563–1566 (2010).
186. Marcinowski, L. et al. Degradation of cellular mir-27 by a novel, highly abundant viral transcript is important for efficient virus replication in vivo. *PLoS Pathog.* **8**, e1002510 (2012).
187. Ghini, F. et al. Endogenous transcripts control miRNA levels and activity in mammalian cells by target-directed miRNA degradation. *Nat. Commun.* **9**, 3119 (2018).
188. de la Mata, M. et al. Potent degradation of neuronal miRNAs induced by highly complementary targets. *EMBO Rep.* https://doi.org/10.15252/embr.201540078 (2015).
189. Ameres, S. L. et al. Target RNA-directed trimming and tailing of small silencing RNAs. *Science* **328**, 1534–1539 (2010).
190. Ameres, S. L. & Zamore, P. D. Diversifying microRNA sequence and function. *Nat. Rev. Mol. Cell Biol.* **14**, 475–488 (2013).
191. Yang, A. et al. AGO-bound mature miRNAs are oligouridylated by TUTs and subsequently degraded by DIS3L2. *Nat. Commun.* **11**, 2765 (2020).
192. Yang, A. et al. TENT2, TUT4, and TUT7 selectively regulate miRNA sequence and abundance. *Nat. Commun.* **13**, 5260 (2022).
193. Shi, C. Y. et al. The ZSWIM8 ubiquitin ligase mediates target-directed microRNA degradation. *Science* https://doi.org/10.1126/science.abc9359 (2020).
194. Han, J. et al. A ubiquitin ligase mediates target-directed microRNA decay independently of tailing and trimming. *Science* https://doi.org/10.1126/science.abc9546 (2020).
Together with Shi et al. (2020), this work reveals the regulatory mechanism of TDMD, via ZSWIM8-mediated Argonaute protein degradation.
195. Piwecka, M. et al. Loss of a mammalian circular RNA locus causes miRNA deregulation and affects brain function. *Science* https://doi.org/10.1126/science.aam8526 (2017).
196. Ulitsky, I., Shkumatava, A., Jan, C. H., Sive, H. & Bartel, D. P. Conserved function of lincRNAs in vertebrate embryonic development despite rapid sequence evolution. *Cell* **147**, 1537–1550 (2011).
197. Kleaveland, B., Shi, C. Y., Stefano, J. & Bartel, D. P. A network of noncoding regulatory RNAs acts in the mammalian brain. *Cell* **174**, 350–362.e17 (2018).
198. Donnelly, B. F. et al. The developmentally timed decay of an essential microRNA family is seed-sequence dependent. *Cell Rep.* **40**, 111154 (2022).
199. Li, L. et al. Widespread microRNA degradation elements in target mRNAs can assist the encoded proteins. *Genes Dev.* **35**, 1595–1609 (2021).
200. Bitetti, A. et al. microRNA degradation by a conserved target RNA regulates animal behavior. *Nat. Struct. Mol. Biol.* **25**, 244–251 (2018).
201. Kingston, E. R., Blodgett, L. W. & Bartel, D. P. Endogenous transcripts direct microRNA degradation in *Drosophila*, and this targeted degradation is required for proper embryonic development. *Mol. Cell* **82**, 3872–3884.e9 (2022).
202. Sheng, P. et al. Screening of Drosophila microRNA-degradation sequences reveals Argonaute1 mRNA's role in regulating miR-999. *Nat. Commun.* **14**, 2108 (2023).
203. Katoh, T. et al. Selective stabilization of mammalian microRNAs by 3′ adenylation mediated by the cytoplasmic poly(A) polymerase GLD-2. *Genes Dev.* **23**, 433–438 (2009).
204. D'Ambrogio, A., Gu, W., Udagawa, T., Mello, C. C. & Richter, J. D. Specific miRNA stabilization by Gld2-catalyzed monoadenylation. *Cell Rep.* https://doi.org/10.1016/j.celrep.2012.10.023 (2012).
205. Jeong, H. C. et al. USB1 is a miRNA deadenylase that regulates hematopoietic development. *Science* **379**, 901–907 (2023).
206. Mansur, F. et al. Gld2-catalyzed 3′ monoadenylation of miRNAs in the hippocampus has no detectable effect on their stability or on animal behavior. *RNA* **22**, 1492–1499 (2016).
207. Vieux, K. F. et al. Screening by deep sequencing reveals mediators of microRNA tailing in *C. elegans*. *Nucleic Acids Res.* **49**, 11167–11180 (2021).
208. Lee, S. et al. Promiscuous splicing-derived hairpins are dominant substrates of tailing-mediated defense of miRNA biogenesis in mammals. *Cell Rep.* **42**, 112111 (2023).
209. Nishida, K. M. et al. Roles of R2D2, a cytoplasmic D2 body component, in the endogenous siRNA pathway in *Drosophila*. *Mol. Cell* **49**, 680–691 (2013).
210. Drake, M. et al. A requirement for ERK dependent Dicer phosphorylation in coordinating oocyte-to-embryo transition in *Caenorhabditis elegans*. *Dev. Cell* **31**, 614–628 (2014).
211. Shang, R. et al. Regulated dicing of pre-mir-144 via reshaping of its terminal loop. *Nucleic acids Res.* **50**, 7637–7654 (2022).
212. Gutierrez-Perez, P. et al. miR-1 sustains muscle physiology by controlling V-ATPase complex assembly. *Sci. Adv.* **7**, eabh1434 (2021).
213. Yang, B., Schwartz, M. & McJunkin, K. In vivo CRISPR screening for phenotypic targets of the mir-35-42 family in *C. elegans*. *Genes Dev.* **34**, 1227–1238 (2020).

214. Ecsedi, M., Rausch, M. & Grosshans, H. The let-7 microRNA directs vulval development through a single target. *Dev. Cell* **32**, 335–344 (2015).
215. Garaulet, D. L., Zhang, B., Wei, L., Li, E. & Lai, E. C. miRNAs and neural alternative polyadenylation specify the virgin behavioral state. *Dev. Cell* **54**, 410–423 (2020).
216. Okamura, K., Hagen, J. W., Duan, H., Tyler, D. M. & Lai, E. C. The mirtron pathway generates microRNA-class regulatory RNAs in *Drosophila*. *Cell* **130**, 89–100 (2007).
217. Ruby, J. G., Jan, C. H. & Bartel, D. P. Intronic microRNA precursors that bypass Drosha processing. *Nature* **448**, 83–86 (2007).
Together with Okamura et al. (2007), this work reports the first non-canonical miRNA pathway, in which intron splicing bypasses Drosha to generate pre-miRNA mimics, termed mirtrons.
218. Bogerd, H. P. et al. A mammalian herpesvirus uses noncanonical expression and processing mechanisms to generate viral microRNAs. *Mol. Cell* **37**, 135–142 (2010).
219. Xie, M. et al. Mammalian 5′-capped microRNA precursors that generate a single microRNA. *Cell* **155**, 1568–1580 (2013).
220. Zamudio, J. R., Kelly, T. J. & Sharp, P. A. Argonaute-bound small RNAs from promoter-proximal RNA polymerase II. *Cell* **156**, 920–934 (2014).
221. Cheloufi, S., Dos Santos, C. O., Chong, M. M. & Hannon, G. J. A dicer-independent miRNA biogenesis pathway that requires Ago catalysis. *Nature* **465**, 584–589 (2010).
222. Cifuentes, D. et al. A novel miRNA processing pathway independent of dicer requires Argonaute2 catalytic activity. *Science* **328**, 1694–1698 (2010).
223. Yang, J. S. et al. Conserved vertebrate mir-451 provides a platform for Dicer-independent, Ago2-mediated microRNA biogenesis. *Proc. Natl Acad. Sci. USA* **107**, 15163–15168 (2010).

Acknowledgements

The authors thank G. La Rocca, B. Kleaveland and L. Joshua-Tor for critical reading, and the referees for informative comments. S.L. was supported by a training award from the NYSTEM contract #C32559GG and the Center for Stem Cell Biology at MSK. Work in E.C.L.'s group was supported by the National Institutes of Health (NIH) (R01-GM083300) and MSK Core Grant P30-CA008748. The authors apologize to those whose work is not included owing to space constraints.

Author contributions

R.S., S.L., G.S. and E.C.L. wrote and edited the manuscript. R.S. S.L. and G.S. drafted the figures. R.S., S.L., G.S. and E.C.L. discussed and reviewed the manuscript before submission.

Competing interests

The authors declare no competing interests.

Additional information

Peer review information *Nature Reviews Genetics* thanks Shuo Gu, Tuan Anh Nguyen, Ian Macrae who co-reviewed with Luca Gebert, and the other, anonymous, reviewer for their contribution to the peer review of this work.